

Stem Cell Reports

Age-related pathological impairments in directly reprogrammed dopaminergic neurons derived from patients with idiopathic Parkinson's disease

--Manuscript Draft--

| | |
|------------------------------|---|
| Manuscript Number: | STEM-CELL-REPORTS-D-21-00493R2 |
| Article Type: | Research Article |
| Keywords: | Induced neurons; induced pluripotent stem cells; Parkinson's disease; direct neural reprogramming; Dopaminergic neurons; autophagy; alpha-synuclein |
| Corresponding Author: | Janelle Drouin-Ouellet University of Montreal Montreal, CANADA |
| First Author: | Janelle Drouin-Ouellet |
| Order of Authors: | Janelle Drouin-Ouellet Emilie M. Legault Fredrik Nilsson Karolina Pircs Julie Bouquety Florence Petit Shelby Shrigley Marcella Birtele Maria Pereira Petter Storm Yogita Sharma Andreas Bruzelius Romina Vuono Malin Kele Thomas B. Stoker Daniella Rylander Ottosson Anna Falk Johan Jakobsson Roger A. Barker Malin Parmar |
| Abstract: | <p>Summary</p> <p>We have developed an efficient approach to generate functional induced dopaminergic (DA) neurons from adult human dermal fibroblasts. When performing DA neuronal conversion of fibroblasts with idiopathic Parkinson's disease (PD), we could specifically detect disease-relevant pathology in these cells. We show that the patient-derived neurons maintain age-related properties of the donor and exhibit lower basal chaperone-mediated autophagy compared to healthy donors. Furthermore, stress-induced autophagy resulted in an age-dependent accumulation of macroautophagic structures. Finally, we show that these impairments in patient-derived DA neurons leads to an accumulation of phosphorylated alpha-synuclein, the classical hallmark of PD pathology. This pathological phenotype is absent in neurons generated from induced pluripotent stem cells from the same patients. Taken together, our results show that direct neural reprogramming can be used for obtaining patient-derived DA</p> |

neurons which uniquely function as a cellular model to study age-related pathology relevant to idiopathic PD.

Age-related pathological impairments in directly reprogrammed dopaminergic neurons derived from patients with idiopathic Parkinson's disease

¹Janelle Drouin-Ouellet^{§*}, ¹Emilie M. Legault[§], ²Fredrik Nilsson, ²Karolina Piracs, ¹Julie Bouquety, ¹Florence Petit, ²Shelby Shrigley, ²Marcella Birtele, ²Maria Pereira, ²Petter Storm, ²Yogita Sharma, ²Andreas Bruzelius, ^{3,4}Romina Vuono, ⁵Malin Kele, ³Thomas B. Stoker, ²Daniella Rylander Ottosson, ⁵Anna Falk, ²Johan Jakobsson, ³Roger A. Barker, and ²Malin Parmar*

¹Faculty of Pharmacy, Université de Montréal, Montreal, Quebec, H3T 1J4, Canada.

²Department of Experimental Medical Science, Wallenberg Neuroscience Center, Division of Neurobiology and Lund Stem Cell Center, Lund University, BMC A11 and B10, S-221 84 Lund, Sweden.

³Wellcome-MRC Cambridge Stem Cell Institute & John van Geest Centre for Brain Repair, Department of Clinical Neurosciences, University of Cambridge, Forvie Site, Cambridge, CB2 0PY.

⁴Medway School of Pharmacy, University of Kent, Chatham Maritime, Chatham, ME4 4TB, UK.

⁵Department of Neuroscience, Karolinska institutet, Stockholm, Sweden

[§]Equal contribution

*Lead contacts : Janelle.drouin-ouellet@umontreal.ca and malin.parmar@med.lu.se

Running title: Pathological impairments in idiopathic PD-iNs

Summary

We have developed an efficient approach to generate functional induced dopaminergic (DA) neurons from adult human dermal fibroblasts. When performing DA neuronal conversion of fibroblasts with idiopathic Parkinson's disease (PD), we could specifically detect disease-relevant pathology in these cells. We show that the patient-derived neurons maintain age-related properties of the donor and exhibit lower basal chaperone-mediated autophagy compared to healthy donors. Furthermore, stress-induced autophagy resulted in an age-dependent accumulation of macroautophagic structures. Finally, we show that these impairments in patient-derived DA neurons leads to an accumulation of phosphorylated alpha-synuclein, the classical hallmark of PD pathology. This pathological phenotype is absent in neurons generated from induced pluripotent stem cells from the same patients. Taken together, our results show that direct neural reprogramming can be used for obtaining patient-derived DA neurons which uniquely function as a cellular model to study age-related pathology relevant to idiopathic PD.

Key words: Induced neurons, induced pluripotent stem cells, Parkinson's disease, direct neural reprogramming, dopaminergic neurons, autophagy, alpha-synuclein

Introduction

Parkinson's disease (PD) is a neurodegenerative disorder that has a major pathology within the midbrain dopaminergic (DA) neurons and involves the aggregation of the misfolded protein alpha-synuclein (α syn). How the disease arises and develops is currently unknown and no cure exists. There is an urgent need for better treatments and disease modifying therapies, but their development is hampered by a poor understanding of the pathogenesis of PD and lack of appropriate model systems, in particular ones which capture age - the biggest risk factor for developing this condition.

In order to better recapitulate disease relevant features and age, we have established a protocol for making induced neurons (iNs) that can be directly generated from adult fibroblasts. This type of direct neural conversion offers several advantages. In particular, such cells retain many important aspects of the ageing signatures of the starting fibroblasts, including age-related changes in the epigenetic clock, the transcriptome and microRNAs, the reactive oxygen species level, DNA damage and telomeres length, as well as in their metabolic profile and mitochondrial defects (Huh et al., 2016; Kim et al., 2018; Mertens et al., 2015; Mertens et al., 2021; Tang et al., 2017; Victor et al., 2018).

The idiopathic nature of most PD cases, coupled to the late age at onset, complicates the study of pathophysiology as it is challenging to design and interpret models of idiopathic PD. For example, animal models depend on toxin-induced mitochondrial damage or overexpression of α syn at non-physiological levels (i.e., levels that exceed what is observed in idiopathic PD patients). Patient-derived induced pluripotent stem cells (iPSCs) are frequently used to study cellular features of PD (Brazdis et al., 2020; Kim et al., 2020; Lang et al., 2019; Yamaguchi et al., 2020) but fail to capture the age and epigenetic signatures of the patient (Kang et al., 2016; Lapasset et al., 2011; Maherali et al., 2007; Mertens et al., 2015; Miller et al., 2013; Tang et al., 2017).

In this study, we investigated iNs (i.e., neurons that are directly generated from fibroblasts) using specific combinations of transcription factors and fate determinants without a pluripotent intermediate (Ambasudhan et al., 2011; Pang et al., 2011) as a mean to better recapitulate disease-relevant features of idiopathic PD. While it is possible to generate iNs with a DA-like phenotype (Caiazzo et al., 2011; Hsu et al., 2014; Jiang et al., 2015; Li et al., 2019; Pereira et al., 2014; Pfisterer et al., 2011; Torper et al., 2013), current protocols are not efficient enough to generate DA neurons from dermal fibroblasts of elderly donors in numbers required for further downstream experimental studies. Therefore, we first identified a combination of reprogramming factors that resulted in the

efficient generation of subtype-specific and functional induced DA neurons (iDANs) when converting dermal fibroblasts from aged individuals. Subsequently, we used this protocol to convert iDANs from idiopathic PD patient-derived fibroblasts as well as age- and sex-matched controls and found that fibroblasts from both healthy controls and idiopathic PD patients converted to functional neurons at similar efficiencies.

When analyzing the patient-derived neurons, we found that stress-induced chaperone-mediated autophagy (CMA) and macroautophagy impairments could be detected in the idiopathic PD iNs but not in control iNs nor in parental fibroblasts of the patients. This type of pathology has previously only been captured in genetic PD variants using iPSC-based models (Sánchez-Danés et al., 2012; Reinhardt et al., 2013; Orenstein et al., 2013; Schöndorf et al., 2014; Fernandes et al., 2016), and we hypothesized that the ability to do so in idiopathic PD iNs as reported here is related to maintenance of donor age in the iNs. To test this, we established iPSCs from a subset of the same patients and used RNA-seq to compare age-related features of iNs derived directly from fibroblasts and iNs derived from cells that had first been reprogrammed through an iPSC intermediary. This analysis confirmed that fibroblast-derived iNs maintain expression of age-associated genes and express mature isoforms of TAU (4R), whereas iPSC-derived iNs do not. In line with this, we were able to detect α syn pathology in directly converted patient-derived neurons but not in iPSC-generated patient-derived neurons. This study thus reports PD-associated phenotypes in directly converted neurons from patient fibroblasts and provides a new model to study idiopathic forms of PD.

Results

Generation of functional iDANs from dermal fibroblasts of adult donors

In order to enable a cell-based model of idiopathic PD using iNs with characteristics of aged DA neurons, we screened 10 different reprogramming factors (*Ascl1*, *Lmx1a*, *Lmx1b*, *FoxA2*, *Otx2*, *Nurr1*, *Smarca1*, *CNPY1*, *EN1*, *PAX8*) that were selected based on their; (i) role during normal DA neurogenesis (Luo and Huang, 2016); (ii) expression in the normal human fetal ventral midbrain (Nelander et al., 2013); (iii) value in predicting functional DA differentiation from human pluripotent stem cells (Kirkeby et al., 2017), and/or (iv) role on midbrain-specific chromatin modeling (Metzakopian et al., 2015). All factors were expressed in combination with the knockdown of the RE1-silencing transcription factor (REST) according to our published protocol for high efficiency reprogramming of adult fibroblasts (Drouin-Ouellet et al., 2017). Three of the screened combinations gave rise to a significant proportion of tyrosine hydroxylase (TH) expressing neurons: shREST +

Ascl1 + Lmx1a/b + FoxA2 + Otx2 (2.21 % \pm 2.02), shREST + Ascl1 + Lmx1a/b + FoxA2 + Otx2 + Smarca1 (7.50 % \pm 3.55), and shREST + Ascl1 + Lmx1a/b + FoxA2 + Otx2 + Nurr1 (**Fig. 1A; Fig. S1A**). The best TH-positive cell yield was obtained with the last combination: shREST + Ascl1 + Lmx1a/b + FoxA2 + Otx2 + Nurr1. This combination gave rise to up to 70.3 % \pm 0.3 of cells expressing the neuronal marker TAU, of which 16.1 % \pm 2.01 also expressed TH (**Fig. S1A**), with an average TAU purity of 9.1% \pm 3.3 and TH purity of 2.6% \pm 1.7 (**Fig. 1B, C**) when reprogramming all lines used in the study (see **Table 1**), and showed robust upregulation of DA genes as measured by RT-qPCR (**Fig. S1B**).

Further characterization of the iNs obtained using this reprogramming factor combination showed that in addition to TH, 35.38% \pm 9.05 of the TAU-positive and 45.20% \pm 14.65 of the MAP2-positive cells were also expressing ALDH1A1 (**Fig. 1D**), which is found in a subset of A9 DA neurons that are more vulnerable to loss in PD (Poulin et al., 2014), as well as VMAT2, a key DA neuronal marker (**Fig. 1E**). Gene expression profiling of 76 neuronal genes relating to dopaminergic, glutamatergic and GABAergic neuronal subtypes confirmed an up-regulation of key genes related to DA patterning and identity (*FOXA1*, *OTX1*, *SHH*, *PITX3*), as well as DA synaptic function - including the receptors *DRD1* to *DRD5*, the DA transporter *DAT*, the enzymes *DDC*, *MAOA*, *ALDH1A1* and the A9-enriched DA marker *GIRK2* (**Fig. 1F; Fig. S1C, D**). Thus the iDANs expressed the key markers of the AT-DAT^{high} subgroup of the DA sublineage as identified in (Tiklová et al., 2019). Finally, to get a better idea of the identity of the cells that did not convert to iNs, we have performed a triple staining using MAP2 to identify iNs, as well as GFAP and Collagen 1 to identify potential glial cells and cells that remained fibroblasts. We observed that some MAP2-negative cells are expressing either Collagen 1 or GFAP alone, or together (**Fig. S1E**).

Morphologically, the iNs are quite immature at this stage (i.e., day 25 to 30), but high-throughput image acquisition analysis showed that TH-positive iNs express significantly more neurites compared to non-TH iNs but had significantly less branch points (**Fig. 1G**). Patch-clamp electrophysiological recordings 65 days post transduction confirmed that the reprogrammed cells had functionally matured (**Fig. 1H**). They were able to fire repetitive action potentials upon injection of current as well as exhibited inward sodium - outward potassium currents with depolarizing steps. When a continuous depolarizing voltage ramp was applied, inward currents was seen across the membrane and could be blocked by the neurotoxin tetrodotoxin (TTX), indicating an involvement of voltage-gated sodium channels in these currents. Without any injection of current or voltage, the cells displayed spontaneous firing and 43.8% of iNs also showed rebound action potentials and/or pacemaker like

activity typical of mesencephalic DA neurons (**Fig. 1H**). Based on this, we refer to the cells as induced DA neurons, iDANs.

Generation of functional iDANs from dermal fibroblasts of idiopathic Parkinson's disease patients

Using this new iDAN reprogramming method, we next converted fibroblasts obtained from skin biopsies of 18 idiopathic PD patients and 10 age- and sex-matched healthy donors (**Table 1**). We found that the fibroblasts obtained from PD patients reprogrammed at a similar efficiency to those obtained from healthy donors (**Fig. 1B**) and displayed a similar neuronal morphological profile (**Fig. 1I, J**). Moreover, when measuring their functional properties using patch clamp electrophysiological recordings, we confirmed that iNs derived from healthy donors (H-iNs) and from PD patients (PD-iNs) displayed similar functionalities in terms of the number of current-induced action potentials, resting membrane potential and the inward sodium - outward potassium currents (**Fig. 1K-M**).

PD-iDANs show altered chaperone-mediated autophagy

To assess the presence of age- and PD-related pathological impairments in iDANs derived from idiopathic PD patients, we focused on autophagy, a lysosomal degradation pathway that is important in cellular homeostasis and the efficiency of which decreases with age (Rubinsztein et al., 2011). We first looked for CMA alterations as this is one type of autophagy that has been suggested to be implicated in the pathophysiology of PD (Cuervo et al., 2004). During CMA, HSC70 recognizes soluble, cytosolic proteins carrying a KFERQ-like motif and guides these proteins to the transmembrane LAMP2a receptor (Galluzzi et al., 2017). Thereafter the protein cargo is translocated into the lysosomal lumen and as such, the level of LAMP2a determines the rate of CMA (Klionsky et al., 2016). To induce autophagy, cells were cultured under starvation conditions, which promotes the recycling of non-essential proteins and organelles for reuse (Klionsky et al., 2021). After validating that the starvation regimen had no impact on the number of neurons and induced changes in LAMP2a and HSC70 expression using western blot (WB) (**Fig. S2A-C**), we assessed CMA expression using a high content imaging approach, which allowed us to analyze cytoplasmic puncta in parental fibroblasts, iNs (TAU-positive and TH-negative) and iDANs (TAU-positive and TH-positive) in a quantitative manner, and also to determine their subcellular location. When investigating this in parental fibroblasts and PD-iNs at baseline and in the context of starvation using an antibody specific to the “a” isoform of LAMP2, we observed a slight reduction in LAMP2a-positive cytoplasmic puncta in healthy donor's parental fibroblasts which was also seen in PD patient's fibroblasts although not significant (**Fig. S3A, B**). Moreover, we did not observe a difference in LAMP2a-positive cytoplasmic puncta in the neurites of TAU-positive iNs upon starvation in both

H-iNs and PD-iNs (**Fig. S4A, B**). However, when looking specifically at iDANs, we observed a lower number of LAMP2a-positive cytoplasmic puncta in the neurites at baseline in the PD-iDANs compared to H-iDANs, suggesting a lower basal rate of CMA in PD-iDANs (**Fig. 2A, B**). Importantly, starvation induced a decrease in LAMP2a-positive cytoplasmic puncta in neurites only in iDANs from the healthy group of donors, suggesting that PD-iDANs have an altered response to starvation, and that this alteration is specific to the DA subtype (**Fig. 2A, B**). We next looked at HSC70 expression, the main chaperone responsible for the degradation of α syn via CMA (Cuervo and Wong, 2014). Both parental fibroblasts from healthy and PD donors showed a decrease in HSC70 expression in response to starvation (**Fig. S3C, D**). While the number of HSC70-positive puncta in the neurites of starved H-iDANs increased (154.0 % \pm 117.2 of the non-starved condition), starvation-induced autophagy led to a decrease of HSC70-positive puncta in PD-iDANs (55.9 % \pm 28.1 of the non-starved condition) (**Fig. 2C, D**). At baseline, an increase in the colocalization between HSC70 and α syn was observed in iDANs from the PD group compared to healthy controls (**Fig. S4F**). However, this was not accompanied by a decrease in α syn in PD-iDANs following starvation (**Fig. S4G, H**). Taken together, and in line with what has been previously reported in animal models of PD (Sala et al., 2016; Xilouri et al., 2016), these results suggest that there is both an alteration in baseline CMA as well as stress-induced autophagy that is specific to idiopathic PD-derived iDANs.

Altered macroautophagy response to stress-induced autophagy in iNs from PD patients

CMA preferentially degrades specific proteins, rather than organelles and other macromolecules (Chiang et al., 1989; Salvador et al., 2000). However, while there is considerable crosstalk between CMA and macroautophagy, starvation predominantly induces macroautophagy - a process involving the formation of double membraned autophagosomes which fuse with lysosomes, resulting in degradation of their contents. Given that we observed CMA alteration in PD-iDANs in response to starvation, we sought to further investigate whether there is an impairment in macroautophagy in PD-iNs. To validate the activation of macroautophagy upon starvation, we first looked at the cargo receptor p62, which decreases in the context of nutrient deprivation (Pircs et al., 2012). In the parental dermal fibroblasts, our starvation regimen induced a decrease in p62-positive cytoplasmic puncta in both healthy- and PD donor-derived lines (**Fig. S5A, B**). This decrease was also observed in H-iNs (70.6 % \pm 27.2 of the non-starved condition in the cell body and 77.1% \pm 22.8 in neurites) (**Fig. 3A, B**). However, once converted to neurons, the majority of PD lines failed to degrade p62 upon starvation, resulting in an accumulation of p62-positive puncta in PD-iNs as compared to H-iNs, which was observed in all TAU-positive iNs, regardless of the neuronal subtype or neuronal

compartment ($97.5 \% \pm 37.1$ of the non-starved condition in the cell body and $106.0\% \pm 37.4$ in neurites) (**Fig. 3A, B**; see representative images of the puncta quantified in **Fig. S6**). We then assessed more specifically LC3 to identify autophagic structures (Pircs et al., 2018). We found that starvation significantly reduced the size of LC3-positive cytoplasmic puncta in the cell bodies of H-iNs ($26.5 \% \pm 15.9$ of the non-starved condition). However, LC3-positive cytoplasmic puncta in the cell body of PD-iNs were not significantly smaller after starvation ($56.5 \% \pm 44.2$ of the non-starved condition). When comparing the level of size reduction of LC3-positive cytoplasmic puncta in the cell body after starvation, PD-iNs failed to reduce puncta size to the level that was seen in the H-iN group (**Fig. 3C, D**), whereas no effect of starvation was observed in the neurites of H-iNs and PD-iNs ($116.3 \% \pm 53.6$ of the non-starved condition for H-iNs, and $104.4 \% \pm 51.8$ for PD-iNs). Furthermore, this difference in macroautophagy between H-iNs and PD-iNs in the cell bodies was a cell type specific feature as it was not seen in the parental fibroblasts (**Fig. S5C, D**).

Once autophagosomes have enclosed their autophagy substrates, they can fuse with endosomes or lysosomes to form amphisomes and autolysosomes. We thus used LAMP2 (detecting all three isoforms: LAMP2a, LAMP2b and LAMP2c) to visualize these structures. LAMP2-positive cytoplasmic puncta decreased upon starvation in the parental fibroblasts of PD lines (**Fig. S5E, F**). However, while an increase of the size of these structures upon starvation was similar in the cell bodies of both H- and PD-iNs ($140.1 \% \pm 41.6$ of the non-starved condition for H-iNs and $130.06 \% \pm 43.8$ for PD-iNs), in the neurites, the size of LAMP2-positive puncta was unaffected by starvation in H-iNs ($118.9 \% \pm 42.3$ of the non-starved condition), whereas they were significantly bigger in PD-iNs ($251.8 \% \pm 177.7$ of the non-starved condition) (**Fig. 3E, F**). Unlike the altered CMA response (**Fig. 2A-C**), these phenotypes were present in all iNs and not just DA neurons (**Fig. S7**). Blocking the autophagic flux by inhibiting the fusion of autophagosomes with lysosomes using Bafilomycin A1 led to an accumulation of LC3-positive puncta in the cell body of H-iNs. However, this accumulation of autophagosomes was absent in PD-iNs (**Fig. S9C-E**), indicating possible impairment at early steps of the autophagic process, as also supported by a downregulation of early autophagy-related genes in PD-iNs (**Fig. S9F**).

To assess whether this altered autophagy response could be due to basal changes in the transcriptome of PD-iNs, we performed RNA-seq analysis on the iNs and the parental fibroblasts. This analysis confirmed there was a major change in gene expression profile as fibroblasts were reprogrammed towards a neuronal phenotype (**Fig. S8**). Moreover, GSEA using KEGG pathways identified genes in the lysosome pathway (hsa014142) to be significantly enriched (adjusted p-value = 0.026) (**Fig**

S9A). When analyzing specifically the lysosomal genes, we found that the lysosomal cholesterol trafficking gene *NCPI* involved in the inherited metabolic disease Niemann-Pick, type C (Park et al., 2003) as well as three other lysosomal enzymes (*NAGA*, *NCSTN*, *NAGLU*) were down-regulated in PD-iNs compared to H-iNs (**Fig. 3G**), supporting the data suggesting that there are alterations in lysosomal functions at baseline and in line with observations that these inherited disorders can lead to parkinsonian states clinically and pathologically (Winder-Rhodes et al., 2012). Importantly, when analyzing expression of these genes between the healthy controls and PD patients in parental fibroblasts, they were not differentially expressed (**Fig. S9B**).

Age-related correlation in disease-associated impairments and accumulation of phosphorylated α syn

Recent reports have shown that age-associated properties of the human donors are maintained in iNs but not in iPSC-derived neurons (Capano et al., 2022); (Huh et al., 2016; Kim et al., 2018; Mertens et al., 2015; Mertens et al., 2021; Tang et al., 2017; Victor et al., 2018). We therefore assessed if the accumulation of lysosomal structures in H- and PD-iNs was associated with the age of the donor. We found a positive correlation between the age and the accumulation of lysosomes in neurites (**Fig. 3H**), and also a trend towards a positive correlation of this accumulation with age of onset at diagnosis (**Fig. 3I**). This was more pronounced in lines derived from patients carrying the H2 haplotype of *MAPT*, which has previously been associated with a more rapid progression and cognitive decline in PD and other neurodegenerative disorders (**Fig. 3J**) (Valenca et al., 2016; Vuono et al., 2015; Williams-Gray et al., 2009; Williams-Gray et al., 2013).

To further study donor age and how this affects disease-related pathology, we next established iPSC lines from the fibroblasts of two patients (with a high amount of pathology as quantified in the iNs derived from same patient's fibroblasts) and 3 controls (see **Table 1**). The cells were reprogrammed into iPSCs using the StemRNA 3rd Generation Reprogramming kit (**Fig. 4A**). QC analysis confirmed that the iPSCs retained a normal karyotype (**Fig. 4B**), and expression of pluripotency markers was confirmed using immunocytochemistry and flow analysis (**Fig. 4C, D**). We then confirmed that the same protocol developed for the fibroblast-to-iDAN conversion (**Fig. 1A**), also converted iPSCs to functional iDANs (**Fig. 4E, F**). iPSC-iDANs expressed high levels of DA-related genes (**Fig. 4G**) and were functionally mature (**Fig. 4H**). Similarly to fibroblast-derived iDANs, there was no differences in neuronal purity, although a slightly lower neurite count was observed in iPSC-derived iDANs from PD patients (**Fig. 4I, J**).

Next, we used RNA-seq from iNs derived from adult fibroblasts (Fib-iNs) and iNs derived from iPSCs (iPSC-iNs) from the same individuals to assess age-related aspects in the resulting neurons (**Fig 5A**). First, GSEA was performed to determine if any molecular features relating to cellular aging were associated with the donor age in Fib-iNs. Genes were ranked based on their association (using Pearson correlation coefficient) with age at sampling and six gene sets related to aging were extracted from the gene ontology database. Despite the limited age span of the donors included in this analysis (58 to 80 years old), we observed a positive correlation between donor age with expression of an age-related gene signature (normalized enrichment score 1.4, adjusted p-value = 0.015) in Fib-iNs (adjusted p-value = 0.4; **Fig 5B-D**). To complement the GSEA data, we also looked at DNA damage, another independent marker of cellular aging, using γ H2AX. This analysis comparing the number of γ H2AX spots in the nucleus of parental fibroblasts with reprogrammed iNs showed a maintenance of the number of γ H2AX spots after 27 days of conversion, which was not the case following reprogramming of these same cell lines to iPSC-iNs, indicating a rejuvenation of the cells during reprogramming to pluripotency (**Fig 5E-G**). Next, we looked at the presence of the isoform of tau that is expressed in adult mature neurons (4R). There are three tau isoforms with 3 repeats (3R) and three isoforms with 4 repeats (4R). These repeats correspond to the protein's binding site to the microtubule of the neuron, making the 4R isoforms binding proteins more stably (Butner and Kirschner, 1991). Neurons generated from iPSCs very strongly express the 3R isoforms but do not express the 4Rs at the protein level, even after one year of in vitro maturation (Iovino et al., 2015; Sposito et al., 2015), reflecting the expression of only the 3Rs of tau at the human embryonic stage (Kosik et al., 1989). In the healthy adult brain, the 3R and 4R isoforms are expressed in a 50/50 ratio (Goedert et al., 1989). This ratio can be substantially altered in neurodegenerative tauopathies. This analysis showed that exon 10 (giving rise to 4R isoforms) is only expressed in iNs from adult fibroblasts (in approximately 40% of the transcripts), and not in iNs derived from fetal fibroblasts (Drouin-Ouellet et al., 2017) or from iPSCs (**Fig 5H**). Moreover, the 3R/4R ratio for adult fibroblasts was 23%, whereas it was <1% for hFL1s. Taken together, this analysis suggests that donor age is at least partially maintained during iN conversion but erased during iPSC reprogramming, similar to other reports (Capano et al., 2022; Mertens et al., 2015; Mertens et al., 2021; Tang et al., 2017; Victor et al., 2018).

Phosphorylated α syn is a hallmark of PD pathology and this has been recapitulated in some iPSC-based cellular models of genetic forms of PD (Kouroupi et al., 2017; Lin et al., 2016) but not idiopathic PD. We therefore sought to investigate whether alterations in stress-induced autophagy observed in Fib-iNs from idiopathic PD patients could lead to changes in the levels of phosphorylated

α syn at the Serine 129 site (pSer129 α syn). No pSer129 α syn staining could be detected in parental fibroblasts. However, we found that while a concurrent activation of macroautophagy by starvation and a blockage of the flux with Bafilomycin A1 did not induce significant changes in pSer129 α syn in H-iNs (83.1 % \pm 53.9 of the starved condition), it did lead to an increase in the number of PD-iNs with pSer129 α syn-positive cytoplasmic dots (126.5 % \pm 54.0 of the starved condition) (**Fig. 6A, B**). This increase in pSer129 α syn-positive cytoplasmic dots was also observed when looking specifically in PD-iDANs as identified with TH staining (128.1% \pm 21.4 of the starved condition), as compared to H-iDANs which again did not show any changes in pSer129 α syn upon Bafilomycin A1 treatment (98.2% \pm 16.0 of the starved condition) (**Fig. 6D, E**). Positive correlation between the accumulation of 81A-positive puncta in two independent experiments evaluating the pSer129 α syn spot expression in iNs and in iDANs shows that the same cell lines are prone to pSer129 α syn accumulation independently of the neuronal subtype, and demonstrates the reproducibility of these experiments (**Fig. S10A**). Interestingly, for some of the results including pSer129 α syn, p62 and LAMP2 accumulation, subanalyses allowed a stratification of the PD patient population based on their age and age at onset (**Fig. S6C** and **Fig. S10C**). Finally, to assess whether elevated basal levels of total α syn could explain the elevated levels of pSer129 α syn observed in lines starved and treated with Bafilomycin A1, we plotted the measure of the total α syn fluorescence intensity against the pSer129 α syn expression measured in iDANs. There was no correlation between basal total α syn levels and the Bafilomycin A1-induced accumulation of pSer129 α syn in iDANs (**Fig. S10B**), suggesting that the increase seen in the PD group is not due to higher basal α syn expression (**Fig. S4C-E**). When assessing iN reprogrammed from iPSCs established from the two PD lines showing the most pSer129 α syn accumulation in fibroblast-derived iNs and iDANs as well as three control lines (**Table 1**), we could not detect any pSer129 α syn puncta in the resulting iPSC-iNs in these lines (**Fig. 6B, C**), supporting that the maintenance of age in iNs is important for modeling the α syn pathophysiology of idiopathic PD.

Discussion

In this study we report on an improved cellular model of idiopathic PD using direct neural conversion of patient fibroblasts. While iDANs have previously been generated from human fibroblasts using several methods (Caiazzo et al., 2011; Hsu et al., 2014; Jiang et al., 2015; Li et al., 2019; Pereira et al., 2014; Pfisterer et al., 2011; Torper et al., 2013), successful reprogramming of adult human dermal

fibroblasts into midbrain DA neurons has only been reported at low efficiency (Caiazzo et al., 2011), making mechanistic studies and disease modeling difficult. Here, we have used a REST knockdown approach to enable neuronal gene transcription in adult cells (Drouin-Ouellet et al., 2017), and combined that with an optimal combination of DA fate determinants (*Lmx1a*, *Lmx1b*, *FoxA2*, *Otx2*, *Nurr1*). This new reprogramming approach increased the efficiency, subtype identity and functional maturation of iDANs during direct conversion, making it possible to perform studies at a scale suitable for disease modeling, drug screening and other biomedical applications. The model is much less labor intensive and cost effective than iPSC-modeling which allowed us to compare iNs from 18 different idiopathic PD patients that were all processed at the same time. Moreover, it maintains the donor's age and reflect pathological changes after only 25 days.

We observed alterations in stress-induced autophagy across the different patient-derived iNs as compared to sex- and age-matched healthy donor lines. We found that blocking the autophagic flux through the inhibition of the fusion of autophagosomes with lysosomes resulted in accumulation of pSer129 α syn in PD-iNs and PD-iDANs. Impairment of autophagy-lysosomal function in iNs derived from PD patients may reflect the effect of the important presence of variants of genes related to lysosomal storage disorders in the PD patient population. Indeed, a recent study reported that more than half of the cases in a PD patient cohort harboured one or more putative damaging variants among the lysosomal storage disorders genes, suggesting the possibility that these variants may interact in a multi-hit, combinatorial manner to degrade lysosomal function, causing the accumulation of α syn and increasing susceptibility to PD (Robak et al., 2017). Future studies using lines derived from patients with strong genetic forms of PD will also help our understanding of the phenotypes found in the idiopathic PD lines and how they relate to different pathways disrupted in familial PD.

Disease-associated impairment could not be detected in the parental fibroblasts, nor in the same cells when they were first reprogrammed to pluripotency and then converted to DA neurons. This shows that direct conversion of fibroblasts, where age-related aspects of the donor are maintained, provides a faithful cell-based model of idiopathic PD. Importantly, our cellular model based on fibroblast-to-neuron conversion showed that iNs from different patients are not impaired to the same degree. Indeed, we found that the degree of impairment relates, at least to some extent, to the age of the donor, the age at onset of their PD and their Tau haplotype. This effect of age and genetic variance on disease pathology has not been recapitulated in cellular models before, and suggests that direct conversion to

iDANs could be used for differential diagnostics, drug screening and disease modeling of late onset neurodegenerative diseases while also capturing the heterogeneity of disease that is apparent clinically.

In this respect, our results demonstrate the utility of establishing models of neurodegenerative disease with cells that resemble the subtype and functionality of the affected neurons in individual patients as closely as possible. For example, we could not detect any autophagy-related impairment in the fibroblasts prior to conversion, clearly demonstrating that the reprogramming to neurons is essential to reveal disease-related phenotypes. Also, specific CMA impairments were detected only in iNs with a DA phenotype.

While it is hard to draw exact parallels between stem-cell derived neurons formed via developmental principles (Hu et al., 2010) and directly converted neurons, both systems have their own merits. Of importance here is that the aging signature of the donor cell is maintained during direct conversion when postmitotic neurons are formed without a proliferative intermediate (Huh et al., 2016; Kim et al., 2018; Mertens et al., 2015; Mertens et al., 2021; Tang et al., 2017; Victor et al., 2018). Our data supports the maintenance of donor age, which uniquely allows for modeling age-related aspects of PD. Future studies using this cellular model will thus contribute to a deeper understanding of the age-associated pathology of PD along with the cellular basis of disease subtypes and variable progression and by so doing allow us to better develop and assess novel therapeutic interventions.

Experimental procedures

Cell lines, genotyping and DNA-sequencing

Adult dermal fibroblasts were obtained from the Parkinson's Disease Research clinic at the John van Geest Centre for Brain Repair (Cambridge, UK) and used under full local ethical approvals: REC 09/H0311/88 (University of Cambridge) and CERSES-18-004-D (University of Montreal) (**Table 1**). The subjects' consent was obtained according to the declaration of Helsinki. Cell lines used in this study will be made available to others subject to appropriate ethical approval and an MTA from the requestor. For biopsy sampling information see (Drouin-Ouellet et al., 2017). All patients were screened for three common Mendelian mutations associated with late onset PD: LRRK2 G2019S as well as GBA L444P and GBA N370S. One out of 19 patients was identified as a LRRK2 G2019S mutation carrier and was removed from further analysis. Samples were also screened for SNCA gene expression levels in our RNA-seq dataset to detect any overexpression of the SNCA gene in the iN samples that would suggest a duplication or triplication. All PD samples included in the RNA-seq

analysis had SNCA expression that followed a normal distribution without any outliers. For MAPT haplotype genotyping, single nucleotide polymorphism (SNP) genotyping was undertaken using a predesigned assay, rs9468 (Applied Biosystems), tagging the MAPT H1 versus H2 haplotype, and run on a Quantstudio 7 Flex Real-Time PCR System (ThermoFisher), according to the manufacturer's instructions. There were no inconsistencies amongst the 28 samples genotyped in triplicates.

Cell culture

Fibroblasts were expanded in T75 flasks with standard fibroblast medium (DMEM, 10 % FBS, 100U/mL penicillin-streptomycin) at 37°C in 5 % CO₂. After thawing, cells were kept for a minimum of two days in culture before starting experiments. When confluent, the cells were dissociated with 0.05 % trypsin and plated at a lower density to expand them. To freeze the fibroblasts from a confluent T75 flask, the cells were detached after 5 minutes incubation in 0.05 % trypsin at 37°C, spun for 5 minutes at 400 g and frozen in a 50/50 mixture of DMEM and FBS with 10 % DMSO. All cell lines were routinely tested for mycoplasma and were negative. For analyses on fibroblasts, cells were plated at a density of 1,900-3,800 cells per cm² in 24-well plates (Nunc) and analyses were performed three days later.

Viral vectors and virus transduction

DNA plasmids expressing mouse open reading frames (ORFs) for *Ascl1*, *Lmx1a*, *Lmx1b*, *FoxA2*, *Otx2*, *Nurr1*, *Smarca1*, *CNPY*, *En1* or *Pax8* in a third-generation lentiviral vector containing a non-regulated ubiquitous phosphoglycerate kinase (PGK) promoter were generated, as well as two short hairpin RNAs (shRNAs) targeting RE1-silencing Transcription Factor (REST) containing a non-regulated U6 promoter. Plasmids used in this study have been deposited in Addgene (#33013, #33014, #34997, #35000, #35001, #127573, #127574). Furthermore, the pB.pA.shREST all-in-one vector from (Birtele et al., 2019; Drouin-Ouellet et al., 2017; Shrigley et al., 2018) was used to reprogram iNs for RNAseq and WB. All the constructs have been verified by sequencing. Lentiviral vectors were produced as previously described (Zufferey et al., 1997) and titrated by qPCR analysis (Georgievska et al., 2004). Transduction was performed at a MOI of 5 for each vector (all viruses used in this study were titered between 1×10^8 and 9×10^9) or MOI of 20 in the case of the pB.pA.shREST vector.

Fibroblast reprogramming to iPSCs

Fibroblasts were cultured in IMDI medium with 10% FBS and 100U/mL penicillin-streptomycin. Fibroblasts were passaged as single cells using TrypLE Select and seeded at a density of 8,000-15,000 cells/cm² on Laminin-521 coated cell culture plates in fibroblast medium. Medium was replaced by Essential E8 medium with 100 U/mL penicillin-streptomycin the day after seeding and thereafter only cultured with E8 medium. Fibroblasts were reprogrammed by using the ReproCELL, StemRNA reprogramming kit. In short, transfection was performed by mixing Lipofectamine RNAiMAX and RNAs provided in the StemRNA kit. Transfection was performed on the hour every 24 hours for four sequential days. Medium was replaced daily, at a minimum 4 hours before transfection. iPSC colonies emerged around day 12-25 post reprogramming and were manually picked for the first passage. Each picked colony was further passaged on as single cells using TrypLE Select. ROCKi at a concentration of 10 µM was added to the Essential 8 medium at each passage. Medium was replaced daily. Quality controls of the generated iPSC colonies were performed from passages 5 and onwards.

Flow analysis

iPSCs were passaged as single cells using TrypLE Select. iPSCs were counted and 200,000-400,000 cells were used for each antibody staining. iPSCs were fixed and permeabilized using the Fixation and Permeabilization buffers according to manufactures instruction (ThermoFisher 00-5523-00). All incubations, fixations and permeabilizations were performed at room temperature. Incubation with antibodies at a concentration of 1 µl/100,000 cells was performed for 30 minutes, at room temperature in the dark. Antibodies provided to separate tubes and unstained cells (without antibody added), were used as negative control. Cells were washed once using Stain buffer before diluted to a concentration of 1 million cell/mL in Stain buffer and passed through a cell strainer before proceeding to Flow analysis. 10,000 events were recorded for each antibody.

Neural reprogramming

For direct neural reprogramming, fibroblasts were plated at a density of 26,300 cells per cm² in 24-well plates (Nunc). Prior to plating, the wells were coated overnight with either 0.1 % gelatin (Sigma), or a combination of PFL for long-term cultures: Polyornithine (15 µg/mL), Fibronectin (0.5 ng/µL) and Laminin (5 µg/mL). Cells used for electrophysiological recordings were directly plated onto glass coverslips coated with PFL as described in (Shrigley et al., 2018). Three days after the viral transduction, the fibroblast medium was replaced with early neural differentiation medium (ENM) (NDiff227; Takara-Clontech) supplemented with growth factors at the following concentrations: LM-22A4 (2 µM, R&D Systems), GDNF (2 ng/mL, R&D Systems), NT3 (10 ng/mL, R&D Systems), as

well as with db-cAMP (0.5 mM, Sigma) and the small molecules CHIR99021 (2 μ M, Axon), SB-431542 (10 μ M, Axon), noggin (0.5 μ g/mL, R&D Systems), LDN-193189 (0.5 μ M, Axon), valproic acid sodium salt (VPA; 1mM, Merck Millipore). Half medium changes were performed twice a week. At 18 days post-transduction, the small molecules were stopped, and the neuronal medium was supplemented only with LM-22A4 (2 μ M), GDNF (2 ng/mL), NT3 (10 ng/mL) and db-cAMP (0.5 mM) until the end of the experiment (Late neuronal medium; LNM). To assess the reprogramming efficiency of each line, all 28 lines were reprogrammed at the same time with the same virus mixture, and this was repeated three times using different batches of virus for each of the 8 lentiviral vectors required for the iDAN reprogramming. For iPSC reprogramming to iDANs, iPSCs were maintained in iPS brew according to (Nolbrant et al., 2017).

Whole cell patch clamp recordings

Prior to recording, the cells on the coverslips were transferred from the culture medium to BrainPhys medium (Bardy et al., 2015) for 30 minutes and maintained at 34.5 °C. Cells were then moved to a recording chamber and submerged in a flowing artificial cerebrospinal fluid (ACSF) solution gassed with 95 % O₂ and 5 % CO₂. The composition of the ACSF was (in mM): 126 NaCl, 2.5 KCl, 1.2 NaH₂PO₄-H₂O, 1.3 MgCl₂-6H₂O, and 2.4 CaCl₂-6H₂O, 22 NaHCO₃, 10 glucose adjusted to pH = 7.4. Temperature of the chamber was maintained at 34 °C throughout the entire recording session. Multi-clamp 700B (Molecular Devices) was used for the recordings and signals were acquired at 10 kHz using pClamp10 software and a data acquisition unit (Digidata 1440A, Molecular Devices). Current was filtered at 0.1 Hz and digitized at 2 kHz. Borosilicate glass pipettes ranging between 4-7 M Ω were used and they were filled with the following intracellular solution (in mM): 122.5 potassium gluconate, 12.5 KCl, 0.2 EGTA, 10 HEPES, 2 MgATP, 0.3 Na₃GTP and 8 NaCl adjusted to pH = 7.3 with KOH as in (Pfisterer et al., 2011). The intracellular solution was kept on ice during the recordings. Cells with neuronal morphology characterized by a rounded cell body were selected for recordings. Input resistances and injected currents were monitored throughout the experiments. Passive properties of the membrane were monitored, and recordings were discarded when changes in the capacitance were higher than 20 % from the beginning to the end of the recording session. Resting membrane potentials were monitored immediately after breaking-in, in current-clamp mode. The membrane potential was kept between -40 mV to -60 mV and currents were injected for 500 ms from -20 pA to +90 pA with 10 pA increments to induce action potentials. The number of action potentials for each cell was taken as the highest frequency of action potential induced by a step of current within the same cell and averaged over the total cells patched per line. Voltage ramp was characterized by constant increase in voltage from -70 mV to +20 mV in 0.5 sec intervals. Inward sodium and delayed

rectifying potassium currents were measured in voltage clamp at depolarizing steps of 10 mV for 100 ms. Spontaneous firing was recorded in voltage-clamp mode at resting membrane potentials. For stem cell-derived iDANs, cells on coverslips were transferred directly to recording chamber with flowing ACSF kept at 34 °C. Membrane potential was kept between -60 mV and -70 mV and currents were injected for 500 ms from -20 pA to +40 pA with 5 pA increments to induce action potentials.

Starvation and Bafilomycin A1 treatment

On day 28 following viral transduction, iNs were starved for 4 hours by replacing the culture medium with HBSS and $\text{Ca}^{2+}/\text{Mg}^{2+}$ and compared to the condition without starvation, where cells were left in their original culture medium. The duration of starvation treatment was chosen based on a starvation curve performed on the iNs (0, 2, 4h), which showed clear increases in p62 and microtubule-associated protein 1 light chain 3 beta, LC3 expression by WB in the absence of neuronal cell death (**Fig. S2D,E**). For the experiment with Bafilomycin A1, cells were starved in HBSS $\text{Ca}^{2+}/\text{Mg}^{2+}$ containing Bafilomycin A1 (100 nM; Sigma Aldrich) for 2 hours and compared to cells incubated in HBSS $\text{Ca}^{2+}/\text{Mg}^{2+}$ containing dimethyl sulfoxide (DMSO; vehicle). This regimen was chosen based on the increase of LC3-II and the LC3-II/LC3-I ratio as assessed by WB. At the end of the incubation period, cells were fixed in 4% paraformaldehyde.

Western blots

Cells were lysed and homogenized as described elsewhere (Pircs et al., 2018). Protein concentration was determined using a DC protein assay kit (Bio-Rad, 5000116). 10-15 µg of protein was boiled at 95°C for 5 min in Laemmli buffer (Bio-Rad), separated on a 4–12 % SDS/PAGE gel and then transferred using the Transblot®-Turbo™ Transfer system (Bio-Rad). After 1 hour blocking in Tris-buffered saline (TBS; 50 mM Tris-Cl, 150 mM NaCl, pH 7.6) with 0.1 % Tween 20 (Sigma-Aldrich, P7949) and 2.5 % (wt:vol) non-fat dry milk (Bio-Rad Laboratories), membranes were incubated overnight at 4°C in one of the primary antibodies summarized in **Table S1**. After washing with TBST, membranes were incubated for 1 hour at room temperature with HRP-conjugated secondary antibodies. Protein expression was developed with the ECL™ Prime Western Blotting Detection Reagent (Life Technologies, RPN2232). Signal was captured using a Chemidoc MP system (Bio-Rad). Band intensity was quantified using ImageJ software (ImageJ, 1.48v) by densitometry.

Immunocytochemistry and high content screening quantifications

Following fixation in 4 % paraformaldehyde, cells were permeabilized with 0.1 % Triton-X-100 in 0.1 M PBS for 10 minutes. Thereafter, cells were blocked for 30 minutes in a solution containing 5

% normal serum in 0.1 M PBS. The primary antibodies used are listed in **Table S1** and were diluted in the blocking solution and applied overnight at 4 °C. Fluorophore-conjugated secondary antibodies (1:200; Jackson ImmunoResearch Laboratories) as well as 4',6-diamidino-2-phenylindole (DAPI; 1:1,000, Sigma Aldrich) were diluted in blocking solution and applied for 2 hours. Fluorescence images of the Heat shock cognate 71 kDa protein (HSC70, also known as HSPA8), lysosome-associated membrane protein 2a (LAMP2a) and tyrosine hydroxylase (TH) and the TAU-81A stainings were taken using a confocal laser scanning microscope (Leica, TCS SP8), whereas the rest of the images were taken using either an inverted microscope (Leica, DFC360 FX-DMI 6000B) or CellInsight CX5 or CX7 High-Content Screening (HCS) microscopes (Thermo Scientific). Images with cells with extreme values were manually verified to make sure that poor focus was not underlying these results (**Fig. S10D**).

The total number of DAPI-positive, TAU-positive and TH-positive cells per well, as well as the average fluorescence intensity for α syn was quantified using the Cellomics Array Scan (Array Scan VTI, Thermo Fischer), which is an automated process ensuring unbiased measurements between groups. Applying the program “Target Activation”, 100-200 fields (10 X magnification) were acquired in a spiral fashion starting from the center, with focus performed on every field of views. The same array, run at 20 X magnification, was used for the analysis of the number of neurites per TAU-positive cell using the program “Neuronal Profiling”. Neuronal purity was calculated as the number of TAU- or MAP2-positive cells over the total number of cells in the well at the end of the experiment. Dopaminergic subtype purity was calculated as the number of TH- or aldehyde dehydrogenase 1 family member A1 (ALDH1A1)-positive cells over the total number of TAU- or MAP2-positive cells in the well at the end of the experiment. Average dot number and size was measured in those neurons in which the cytoplasm and neurites were defined by TAU or TH staining. Puncta of p62, LC3, LAMP2, LAMP2a, HSC70, α syn and 81A were detected (using a “Spot Detection” program) and measured in each case. For each neuron identified by the software based on TAU/MAP2 and TH expression, the number and size of puncta in the cell body and neurites were measured using an isodata thresholding method. The data is presented as the average number or size of dots detected per cell in each compartment. Experiments done on fibroblasts were quantified using the same approach, with quantification of puncta of p62, LC3, LAMP2, LAMP2a and HSC70 in the cytoplasm, defined by vimentin (VIM)-positive staining. For γ H2AX measurements, puncta positive for γ H2AX were detected in the nuclei of fibroblasts and iDANs (defined by the DAPI stained region) at 20 X magnification using a “Spot Detection” program. Cell images in **Fig. 2, Fig. 3A, C, E** and

Fig. 6A, B, E were representative images acquired by confocal microscopy (Zeiss LSM800) at 63X.

qRT-PCR for neuronal gene expression

Total RNA was extracted from human fibroblasts as well as iNs from the same lines using the miRNeasy kit (Qiagen) followed by Universal cDNA synthesis kit (Fermentas). Three reference genes were used for each qPCR analysis (ACTB, GAPDH and HPRT1). All primers were used together with LightCycler 480 SYBR Green I Master (Roche). Standard procedures of qRT-PCR were used, and data quantified using the $\Delta\Delta C_t$ -method. Statistical analyses were performed on triplicates. A custom RT² profiler PCR Array (Qiagen) containing 90 neuronal genes was also used according to the manufacturer instructions.

RNA-seq analysis

Fibroblasts from the healthy donor (n = 10) and PD (n = 10) lines were plated and either collected for RNA extraction following 3 days in culture or transduced with the pB.pA.shREST lentiviral vector (Birtele et al., 2019; Drouin-Ouellet et al., 2017; Shrigley et al., 2018) the day following plating and allowed to be reprogrammed for 30 days. RNA was extracted using the RNeasy mini kit (Qiagen) with DNase treatment. cDNA libraries were prepared using the Illumina truseq library preparation kit and sequenced with 2 x 150 bp paired end reads on an Illumina NextSeq 500 High Output kit. For iPSC-iDANs cDNA libraries were generated using Smart-seq2 (Takara). Raw base calls were demultiplexed and converted into sample specific fastq format files using default parameters of the bcl2fastq program provided by illumina. Quality of reads was checked using FastQC and multiQC tools. Reads were mapped to the human genome (GRCh37) using the STAR mapping algorithm (Dobin et al., 2013). mRNA expression was quantified using RSEM (Li and Dewey, 2011). Downstream analyses were performed using in house R scripts. Gene Set Enrichment Analysis was performed by fitting a linear model, adjusting for sex and disease status as covariates, and genes were ranked based on their association with age at sampling. Six gene sets related to aging were extracted from the gene ontology database and queried using GSEA (as implemented in the clusterProfiler R package). Differential splicing of the MAPT gene was visualized in IGV (version 2.8). Significant up and down regulated pathways were selected using Bonferroni post hoc corrected p values ($p_{adj} < 1e-4$).

Statistical analysis

All data are expressed as mean \pm the standard deviation. Whenever the analysis is performed with

one cell line, biological replicates ($n = 3-4$) were used. In case of experiments using multiple cell lines, we used a minimum of $n = 6$ to account for inter-individual variation. A Shapiro-Wilk normality test was used to assess the normality of the distribution. When a normal distribution could not be assumed, a non-parametric test was performed. Groups were compared using a one-way ANOVA with a Bonferroni post hoc or a Kruskal-Wallis test with a Dunn's multiple comparisons tests. To determine whether there was a significant difference between two sets of observations repeated on the same lines, a paired sample t-test was also performed. In case of only two groups, they were compared using a Student *t*-test. An F test was used to compare variance and in case of unequal variance a Welch's correction test was then performed. Statistical analyses were conducted using the GraphPad Prism 7.0. An alpha level of $p < 0.05$ was set for significance.

Data availability

The RNAseq dataset can be found on the GEO repository under accession number GSE125239.

Acknowledgements

We thank Marie Persson Vejgård, Sol Da Rocha Baez, Ulla Jarl (Lund University), and Dr. Maria Ban (Neurology Unit at the University of Cambridge) for technical assistance as well as Dr. Anna Hammarberg at the MultiPark Cellomics platform at Lund University for her valuable help with high content imaging.

Funding

The research leading to these results has received funding from the New York Stem Cell Foundation, the European Research Council under the European Union's Seventh Framework Programme: FP/2007-2013 NeuroStemcellRepair (no. 602278) and ERC Grant Agreement no. 771427, the Swedish Research Council (grant agreement 2016-00873), Swedish Parkinson Foundation (Parkinsonfonden), Hjärnfonden (FO2019-0301), Olle Engkvist Foundation 203-0006 (JJ), the Strategic Research Areas at Lund University MultiPark (Multidisciplinary research in Parkinson's disease) and StemTherapy, the Cure Parkinson's Trust in the UK and Parkinson Canada (2018-00236) (J. D.-O). This research was also supported by the Canada Research Chair Program and the NIHR Cambridge Biomedical Research Centre (BRC-1215-20014). The views expressed are those of the author(s) and not necessarily those of the NIHR or the Department of Health and Social Care. This research was funded in part by the Wellcome Trust 203151/Z/16/Z. For the purpose of Open Access, the author has applied a CC BY public copyright licence to any Author Accepted Manuscript version arising from this submission. RAB was a NIHR Senior Investigator. M.P. is a New York Stem Cell Foundation - Robertson Investigator. J. D.-O. is a Canada Research Chair and received support from FRQS in partnership with Parkinson Québec (#268980) and the Canada Foundation for Innovation (#38354). M.B and S.S were funded by the European Union Horizon 2020 Programme (H2020-MSCA-ITN-2015) under the Marie Skłodowska-Curie Innovative Training Network and Grant Agreement No. 676408. E. M. L. is supported by a FRQS Graduate Scholarship in partnership with Parkinson Canada.

Competing interests

M.Pa., J.J. and J.DO. are co-inventors of the patent application PCT/EP2018/ 062261 owned by New York Stem Cell Foundation. M.Pa is the owner of Parmar Cells AB.

Author contributions

J.D.-O., K.P., J.J., R.A.B. and M.Pa. designed research; J.D.-O., E.M.L., F.N., K.P., J.B., F.P., M.B., S.S., M.Pe., A.B., M. K., R.V. T.S. and K.P. performed research; D.R. O., A.F. and R.A.B. contributed new reagents/analytic tools; J.D.-O., E.M.L., F.N., K.P., J.B., F.P., M.B., S.S., P.S., Y.S., R.V. and K.P Analyzed data; J.D.-O. and M.Pa. wrote the first draft of the paper.

References

- Ambasudhan, R., Talantova, M., Coleman, R., Yuan, X., Zhu, S., Lipton, S. A., and Ding, S. (2011). Direct reprogramming of adult human fibroblasts to functional neurons under defined conditions. *Cell Stem Cell* 9, 113-118.
- Bardy, C. et al. (2015). Neuronal medium that supports basic synaptic functions and activity of human neurons in vitro. *Proc Natl Acad Sci U S A* 112, E2725-34.
- Birtele, M., Sharma, Y., Kidnapillai, S., Lau, S., Stoker, T. B., Barker, R. A., Rylander Ottosson, D., Drouin-Ouellet, J., and Parmar, M. (2019). Dual modulation of neuron-specific microRNAs and the REST complex promotes functional maturation of human adult induced neurons. *FEBS Lett* 593, 3370-3380.
- Brazdis, R. M. et al. (2020). Demonstration of brain region-specific neuronal vulnerability in human iPSC-based model of familial Parkinson's disease. *Hum Mol Genet* 29, 1180-1191.
- Butner, K. A., and Kirschner, M. W. (1991). Tau protein binds to microtubules through a flexible array of distributed weak sites. *J Cell Biol* 115, 717-730.
- Caiazzo, M. et al. (2011). Direct generation of functional dopaminergic neurons from mouse and human fibroblasts. *Nature* 476, 224-227.
- Capano, L. S. et al. (2022). Recapitulation of endogenous 4R tau expression and formation of insoluble tau in directly reprogrammed human neurons. *Cell Stem Cell* 29, 918-932.e8.
- Chiang, H. L., Terlecky, S. R., Plant, C. P., and Dice, J. F. (1989). A role for a 70-kilodalton heat shock protein in lysosomal degradation of intracellular proteins. *Science* 246, 382-385.
- Cuervo, A. M., Stefanis, L., Fredenburg, R., Lansbury, P. T., and Sulzer, D. (2004). Impaired degradation of mutant alpha-synuclein by chaperone-mediated autophagy. *Science* 305, 1292-1295.
- Cuervo, A. M., and Wong, E. (2014). Chaperone-mediated autophagy: roles in disease and aging. *Cell Res* 24, 92-104.
- Dobin, A., Davis, C. A., Schlesinger, F., Drenkow, J., Zaleski, C., Jha, S., Batut, P., Chaisson, M., and Gingeras, T. R. (2013). STAR: ultrafast universal RNA-seq aligner. *Bioinformatics* 29, 15-21.
- Drouin-Ouellet, J. et al. (2017). REST suppression mediates neural conversion of adult human fibroblasts via microRNA-dependent and -independent pathways. *EMBO Mol Med* 9, 1117-1131.
- Fernandes, H. J. et al. (2016). ER Stress and Autophagic Perturbations Lead to Elevated Extracellular α -Synuclein in GBA-N370S Parkinson's iPSC-Derived Dopamine Neurons. *Stem Cell Reports* 6, 342-356.
- Galluzzi, L. et al. (2017). Molecular definitions of autophagy and related processes. *EMBO J* 36, 1811-1836.

- Georgievska, B., Jakobsson, J., Persson, E., Ericson, C., Kirik, D., and Lundberg, C. (2004). Regulated delivery of glial cell line-derived neurotrophic factor into rat striatum, using a tetracycline-dependent lentiviral vector. *Hum Gene Ther* 15, 934-944.
- Goedert, M., Spillantini, M. G., Jakes, R., Rutherford, D., and Crowther, R. A. (1989). Multiple isoforms of human microtubule-associated protein tau: sequences and localization in neurofibrillary tangles of Alzheimer's disease. *Neuron* 3, 519-526.
- Hsu, Y. C., Chen, S. L., Wang, Y. J., Chen, Y. H., Wang, D. Y., Chen, L., Chen, C. H., Chen, H. H., and Chiu, I. M. (2014). Signaling adaptor protein SH2B1 enhances neurite outgrowth and accelerates the maturation of human induced neurons. *Stem Cells Transl Med* 3, 713-722.
- Hu, B. Y., Weick, J. P., Yu, J., Ma, L. X., Zhang, X. Q., Thomson, J. A., and Zhang, S. C. (2010). Neural differentiation of human induced pluripotent stem cells follows developmental principles but with variable potency. *Proc Natl Acad Sci U S A* 107, 4335-4340.
- Huh, C. J., Zhang, B., Victor, M. B., Dahiya, S., Batista, L. F., Horvath, S., and Yoo, A. S. (2016). Maintenance of age in human neurons generated by microRNA-based neuronal conversion of fibroblasts. *Elife* 5,
- Iovino, M. et al. (2015). Early maturation and distinct tau pathology in induced pluripotent stem cell-derived neurons from patients with MAPT mutations. *Brain* 138, 3345-3359.
- Jiang, H. et al. (2015). Cell cycle and p53 gate the direct conversion of human fibroblasts to dopaminergic neurons. *Nat Commun* 6, 10100.
- Kang, E. et al. (2016). Age-Related Accumulation of Somatic Mitochondrial DNA Mutations in Adult-Derived Human iPSCs. *Cell Stem Cell* 18, 625-636.
- Kim, J. W. et al. (2020). Defects in mRNA Translation in LRRK2-Mutant hiPSC-Derived Dopaminergic Neurons Lead to Dysregulated Calcium Homeostasis. *Cell Stem Cell* 27, 633-645.e7.
- Kim, Y. et al. (2018). Mitochondrial Aging Defects Emerge in Directly Reprogrammed Human Neurons due to Their Metabolic Profile. *Cell Rep* 23, 2550-2558.
- Kirkeby, A. et al. (2017). Predictive Markers Guide Differentiation to Improve Graft Outcome in Clinical Translation of hESC-Based Therapy for Parkinson's Disease. *Cell Stem Cell* 20, 135-148.
- Klionsky, D. J., Abdel-Aziz, A. K., Abdelfatah, S., Abdellatif, M., Abdoli, A., Abel, S., Abeliovich, H., Abildgaard, M. H., Abudu, Y. P., and Acevedo-Arozena, A. (2021). Guidelines for the use and interpretation of assays for monitoring autophagy. *autophagy* 1-382.
- Klionsky, D. J. et al. (2016). Guidelines for the use and interpretation of assays for monitoring autophagy (3rd edition). *Autophagy* 12, 1-222.
- Kosik, K. S., Orecchio, L. D., Bakalis, S., and Neve, R. L. (1989). Developmentally regulated expression of specific tau sequences. *Neuron* 2, 1389-1397.
- Kouroupi, G. et al. (2017). Defective synaptic connectivity and axonal neuropathology in a human iPSC-based model of familial Parkinson's disease. *Proc Natl Acad Sci U S A* 114, E3679-E3688.

- Lang, C. et al. (2019). Single-Cell Sequencing of iPSC-Dopamine Neurons Reconstructs Disease Progression and Identifies HDAC4 as a Regulator of Parkinson Cell Phenotypes. *Cell Stem Cell* *24*, 93-106.e6.
- Lapasset, L. et al. (2011). Rejuvenating senescent and centenarian human cells by reprogramming through the pluripotent state. *Genes Dev* *25*, 2248-2253.
- Li, B., and Dewey, C. N. (2011). RSEM: accurate transcript quantification from RNA-Seq data with or without a reference genome. *BMC Bioinformatics* *12*, 323.
- Li, H., Jiang, H., Yin, X., Bard, J. E., Zhang, B., and Feng, J. (2019). Attenuation of PRRX2 and HEY2 enables efficient conversion of adult human skin fibroblasts to neurons. *Biochem Biophys Res Commun* *516*, 765-769.
- Lin, L., Göke, J., Cukuroglu, E., Dranias, M. R., VanDongen, A. M., and Stanton, L. W. (2016). Molecular Features Underlying Neurodegeneration Identified through In Vitro Modeling of Genetically Diverse Parkinson's Disease Patients. *Cell Rep* *15*, 2411-2426.
- Luo, S. X., and Huang, E. J. (2016). Dopaminergic Neurons and Brain Reward Pathways: From Neurogenesis to Circuit Assembly. *Am J Pathol* *186*, 478-488.
- Maherali, N. et al. (2007). Directly reprogrammed fibroblasts show global epigenetic remodeling and widespread tissue contribution. *Cell Stem Cell* *1*, 55-70.
- Mertens, J. et al. (2021). Age-dependent instability of mature neuronal fate in induced neurons from Alzheimer's patients. *Cell Stem Cell* S1934-5909(21)00161.
- Mertens, J. et al. (2015). Directly Reprogrammed Human Neurons Retain Aging-Associated Transcriptomic Signatures and Reveal Age-Related Nucleocytoplasmic Defects. *Cell Stem Cell* *17*, 705-718.
- Metzakopian, E., Bouhali, K., Alvarez-Saavedra, M., Whitsett, J. A., Picketts, D. J., and Ang, S. L. (2015). Genome-wide characterisation of Foxa1 binding sites reveals several mechanisms for regulating neuronal differentiation in midbrain dopamine cells. *Development* *142*, 1315-1324.
- Miller, J. D. et al. (2013). Human iPSC-based modeling of late-onset disease via progerin-induced aging. *Cell Stem Cell* *13*, 691-705.
- Nelander, J., Grealish, S., and Parmar, M. (2013). Human foetal brain tissue as quality control when developing stem cells towards cell replacement therapy for neurological diseases. *Neuroreport* *24*, 1025-1030.
- Nolbrant, S., Heuer, A., Parmar, M., and Kirkeby, A. (2017). Generation of high-purity human ventral midbrain dopaminergic progenitors for in vitro maturation and intracerebral transplantation. *Nat Protoc* *12*, 1962-1979.
- Orenstein, S. J. et al. (2013). Interplay of LRRK2 with chaperone-mediated autophagy. *Nat Neurosci* *16*, 394-406.

- Pang, Z. P. et al. (2011). Induction of human neuronal cells by defined transcription factors. *Nature* 476, 220-223.
- Park, W. D., O'Brien, J. F., Lundquist, P. A., Kraft, D. L., Vockley, C. W., Karnes, P. S., Patterson, M. C., and Snow, K. (2003). Identification of 58 novel mutations in Niemann-Pick disease type C: correlation with biochemical phenotype and importance of PTC1-like domains in NPC1. *Hum Mutat* 22, 313-325.
- Pereira, M., Pfisterer, U., Rylander, D., Torper, O., Lau, S., Lundblad, M., Grealish, S., and Parmar, M. (2014). Highly efficient generation of induced neurons from human fibroblasts that survive transplantation into the adult rat brain. *Sci Rep* 4, 6330.
- Pfisterer, U., Kirkeby, A., Torper, O., Wood, J., Nelander, J., Dufour, A., Bjorklund, A., Lindvall, O., Jakobsson, J., and Parmar, M. (2011). Direct conversion of human fibroblasts to dopaminergic neurons. *Proc Natl Acad Sci U S A* 108, 10343-10348.
- Pircs, K., Nagy, P., Varga, A., Venkei, Z., Erdi, B., Hegedus, K., and Juhasz, G. (2012). Advantages and limitations of different p62-based assays for estimating autophagic activity in *Drosophila*. *PLoS One* 7, e44214.
- Pircs, K. et al. (2018). Huntingtin Aggregation Impairs Autophagy, Leading to Argonaute-2 Accumulation and Global MicroRNA Dysregulation. *Cell Rep* 24, 1397-1406.
- Poulin, J. F., Zou, J., Drouin-Ouellet, J., Kim, K. Y., Cicchetti, F., and Awatramani, R. B. (2014). Defining midbrain dopaminergic neuron diversity by single-cell gene expression profiling. *Cell Rep* 9, 930-943.
- Reinhardt, P. et al. (2013). Genetic correction of a LRRK2 mutation in human iPSCs links parkinsonian neurodegeneration to ERK-dependent changes in gene expression. *Cell Stem Cell* 12, 354-367.
- Robak, L. A., Jansen, I. E., van Rooij, J., Uitterlinden, A. G., Kraaij, R., Jankovic, J., International Parkinson's Disease Genomics Consortium, I. P. D. G. C., Heutink, P., and Shulman, J. M. (2017). Excessive burden of lysosomal storage disorder gene variants in Parkinson's disease. *Brain* 140, 3191-3203.
- Rubinsztein, D. C., Mariño, G., and Kroemer, G. (2011). Autophagy and aging. *Cell* 146, 682-695.
- Sala, G., Marinig, D., Arosio, A., and Ferrarese, C. (2016). Role of Chaperone-Mediated Autophagy Dysfunctions in the Pathogenesis of Parkinson's Disease. *Front Mol Neurosci* 9, 157.
- Salvador, N., Aguado, C., Horst, M., and Knecht, E. (2000). Import of a cytosolic protein into lysosomes by chaperone-mediated autophagy depends on its folding state. *J Biol Chem* 275, 27447-27456.
- Sánchez-Danés, A. et al. (2012). Disease-specific phenotypes in dopamine neurons from human iPSC-based models of genetic and sporadic Parkinson's disease. *EMBO Mol Med* 4, 380-395.
- Schöndorf, D. C. et al. (2014). iPSC-derived neurons from GBA1-associated Parkinson's disease patients show autophagic defects and impaired calcium homeostasis. *Nat Commun* 5, 4028.

- Shrigley, S., Piracs, K., Barker, R. A., Parmar, M., and Drouin-Ouellet, J. (2018). Simple Generation of a High Yield Culture of Induced Neurons from Human Adult Skin Fibroblasts. *J Vis Exp* (132) 56904.
- Sposito, T. et al. (2015). Developmental regulation of tau splicing is disrupted in stem cell-derived neurons from frontotemporal dementia patients with the 10 + 16 splice-site mutation in MAPT. *Hum Mol Genet* 24, 5260-5269.
- Tang, Y., Liu, M. L., Zang, T., and Zhang, C. L. (2017). Direct Reprogramming Rather than iPSC-Based Reprogramming Maintains Aging Hallmarks in Human Motor Neurons. *Front Mol Neurosci* 10, 359.
- Tiklová, K. et al. (2019). Single-cell RNA sequencing reveals midbrain dopamine neuron diversity emerging during mouse brain development. *Nat Commun* 10, 581.
- Torper, O., Pfisterer, U., Wolf, D. A., Pereira, M., Lau, S., Jakobsson, J., Björklund, A., Grealish, S., and Parmar, M. (2013). Generation of induced neurons via direct conversion in vivo. *Proc Natl Acad Sci U S A* 110, 7038-7043.
- Valenca, G. T., Srivastava, G. P., Oliveira-Filho, J., White, C. C., Yu, L., Schneider, J. A., Buchman, A. S., Shulman, J. M., Bennett, D. A., and De Jager, P. L. (2016). The Role of MAPT Haplotype H2 and Isoform 1N/4R in Parkinsonism of Older Adults. *PLoS One* 11, e0157452.
- Victor, M. B. et al. (2018). Striatal neurons directly converted from Huntington's disease patient fibroblasts recapitulate age-associated disease phenotypes. *Nat Neurosci* 21, 341-352.
- Vuono, R., Winder-Rhodes, S., de Silva, R., Cisbani, G., Drouin-Ouellet, J., REGISTRY, I. O. T. E. H. D. N., Spillantini, M. G., Cicchetti, F., and Barker, R. A. (2015). The role of tau in the pathological process and clinical expression of Huntington's disease. *Brain* 138, 1907-1918.
- Williams-Gray, C. H. et al. (2009). The distinct cognitive syndromes of Parkinson's disease: 5 year follow-up of the CamPaIGN cohort. *Brain* 132, 2958-2969.
- Williams-Gray, C. H., Mason, S. L., Evans, J. R., Foltynie, T., Brayne, C., Robbins, T. W., and Barker, R. A. (2013). The CamPaIGN study of Parkinson's disease: 10-year outlook in an incident population-based cohort. *J Neurol Neurosurg Psychiatry* 84, 1258-1264.
- Winder-Rhodes, S. E. et al. (2012). Genetic and pathological links between Parkinson's disease and the lysosomal disorder Sanfilippo syndrome. *Mov Disord* 27, 312-315.
- Xilouri, M., Brekk, O. R., Polissidis, A., Chrysanthou-Piterou, M., Kloukina, I., and Stefanis, L. (2016). Impairment of chaperone-mediated autophagy induces dopaminergic neurodegeneration in rats. *Autophagy* 12, 2230-2247.
- Yamaguchi, A. et al. (2020). Identifying Therapeutic Agents for Amelioration of Mitochondrial Clearance Disorder in Neurons of Familial Parkinson Disease. *Stem Cell Reports* 14, 1060-1075.
- Zufferey, R., Nagy, D., Mandel, R. J., Naldini, L., and Trono, D. (1997). Multiply attenuated lentiviral vector achieves efficient gene delivery in vivo. *Nat Biotechnol* 15, 871-875.

Figure legends

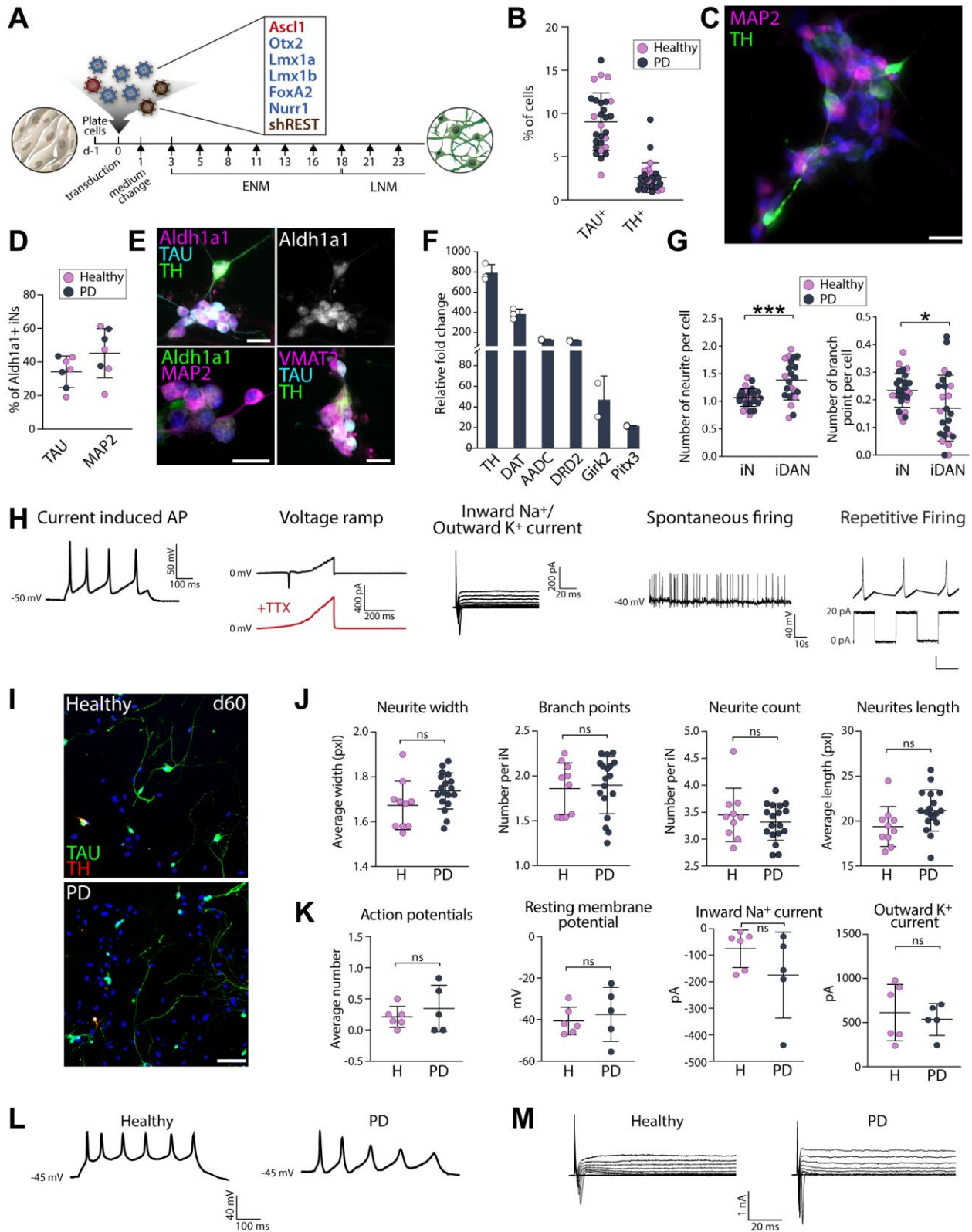


Figure 1. Generation of iDANs from Parkinson's disease and healthy donor lines.

(A) Reprogramming iDANs from adult fibroblasts.

(B) Quantification of TAU-positive and TH-positive cells (mean average of 2,575 TAU-positive and 32 TH-positive cells assessed per line, n=28 lines).

(C) TAU-positive and TH-positive iDANs. Cells are counterstained with DAPI (in blue). Scale bar = 25µm.

(D) Quantification of ALDH1A1 and TAU or MAP2 double positive cells (mean average of 1,652 TAU-positive and 1,258 MAP2-positive cells assessed per well from 4 biological replicates per lines, n=7 lines (lines #4, #8, #9, #10, #26, #27 and #28)).

(E) TAU-positive, MAP2-positive and TH-positive iNs and iDANs expressing ALDH1A1 and VMAT2. Cells are counterstained with DAPI (in blue). Scale bars = 25µm.

(F) Gene expression quantification of DA genes relative to parental fibroblast levels (from 2 to 3 biological replicates (white dots) from line #2).

(G) Quantification of the neurite profile in TAU-positive and TH-negative (iNs) vs. TAU and TH double positive cells (iDANs) from healthy and Parkinson's disease lines (mean average of 2,575 TAU-positive and 32 TH-positive cells assessed per line, n=28 lines). Two-tailed unpaired t-test with Welch's correction: ***P=0.0004, df=30.82; *P=0.0245, df=32.94.

(H) Patch clamp recordings of iDANs from line #2 (at day 65).

(I) Double TAU-positive and TH-positive H-iDANs and PD-iDANs at day 60. Scale bar = 100µm.

(J) Quantification of the neurite profile in TAU-positive H-iNs and PD-iNs (experiment has been repeated independently 3 times, mean average of 2,142 TAU-positive cells assessed per line, n=10 healthy and n=18 Parkinson's disease lines).

(K) Quantification of voltage-clamp recordings of evoked action potentials ($n = 8-10$ neurons per lines, $n = 5-6$ lines per group), resting membrane potential of H-iNs and PD-iNs. ($n = 4-9$ neurons per lines, $n = 5-6$ lines per group), inward and outward currents ($n = 4-9$ neurons per lines, $n = 5-6$ lines per group). Lines #1, #2, #4, #5, #6, #8, #13, #16, #17, #24, #28 were used for patch clamp experiments.

(L) Voltage-clamp recordings of repetitive evoked action potentials.

(M) Representative traces of membrane sodium- and potassium currents following voltage depolarization steps in H-iNs and PD-iNs.

Abbreviations: APs: action potentials, ns: not significant, TTX: tetrodotoxin.

Table 1. Demographics, clinical and genotype data of the study participants.

| Line ID | Group | Sex | Age at biopsy | MAPT haplotype | Age at onset | Disease duration (years) | *UPDRS motor decline | *MMSE score decline | iPSC lines |
|---------|-----------------------|------|---------------|----------------|--------------|--------------------------|----------------------|---------------------|------------|
| 1 | Healthy | M | 69 | H1/H1 | | | | | |
| 2 | Healthy | F | 67 | H1/H1 | | | | | |
| 3 | Healthy | M | 80 | H2/H2 | | | | | |
| 4 | Healthy | F | 75 | H1/H1 | | | | | Healthy 4 |
| 5 | Healthy | M | 70 | H1/H2 | | | | | Healthy 5 |
| 6 | Healthy | F | 70 | H1/H2 | | | | | |
| 7 | Healthy | M | 71 | H1/H1 | | | | | |
| 8 | Healthy | F | 61 | H1/H2 | | | | | Healthy 8 |
| 9 | Healthy | F | 66 | H2/H2 | | | | | |
| 10 | Healthy | F | 58 | H1/H1 | | | | | |
| | Ratio F:M/ Mean±SD | 6:4 | 68.7 ± 6.3 | | | | | | |
| 11 | PD | M | 56 | H1/H1 | 34 | 23 | -0.32 | 0 | |
| 12 | PD | M | 60 | H1/H1 | 48 | 12 | -0.43 | 0 | |
| 13 | PD | F | 77 | H2/H2 | 65 | 12 | 1.48 | 0 | |
| 14 | PD | F | 67 | H1/H1 | 56 | 12 | 0.76 | -0.07 | |
| 15 | PD | F | 59 | H1/H1 | 45 | 15 | -1.39 | 0 | |
| 16 | PD | F | 80 | H1/H2 | 69 | 11 | 0.39 | -0.07 | |
| 17 | PD | M | 80 | H2/H2 | 49 | 33 | 1.70 | 0 | |
| 18 | PD | F | 87 | H1/H1 | 72 | 15 | 0.25 | -0.12 | |
| 19 | PD | F | 77 | H1/H1 | 56 | 24 | -0.42 | -0.25 | |
| 20 | PD | M | 75 | H1/H1 | 63 | 13 | -1.18 | 0 | |
| 21 | PD | M | 77 | H1/H1 | 66 | 11 | -1.68 | 0 | |
| 22 | PD | F | 71 | H1/H1 | 62 | 14 | 0 | -0.47 | |
| 23 | PD | M | 72 | H1/H1 | 70 | 2 | 1.71 | -0.44 | |
| 24 | PD | M | 81 | H1/H1 | 76 | 6 | 1.88 | 0.14 | |
| 25 | PD | F | 44 | H1/H1 | 40 | 5 | -3.56 | 0.15 | |
| 26 | PD | F | 79 | H1/H1 | NA | NA | NA | NA | PD 26 |
| 27 | PD | F | 68 | H1/H1 | 55 | 15 | 1.65 | 0 | |
| 28 | PD | M | 57 | H1/H1 | 50 | 8 | NA | NA | PD 28 |
| | Ratio F:M/ Mean±SD | 10:8 | 70.4 ± 11.2 | | 57.4 ± 11.9 | 12.5 ± 7.1 | 0.05 ± 1.5 | -0.07± 0.18 | |

* Average rate of decline per year over a minimum of 2 years.

Abbreviations: MMSE: Mini-Mental State Examination; NA: not available; UPDRS: Unified Parkinson's Disease Rating Scale

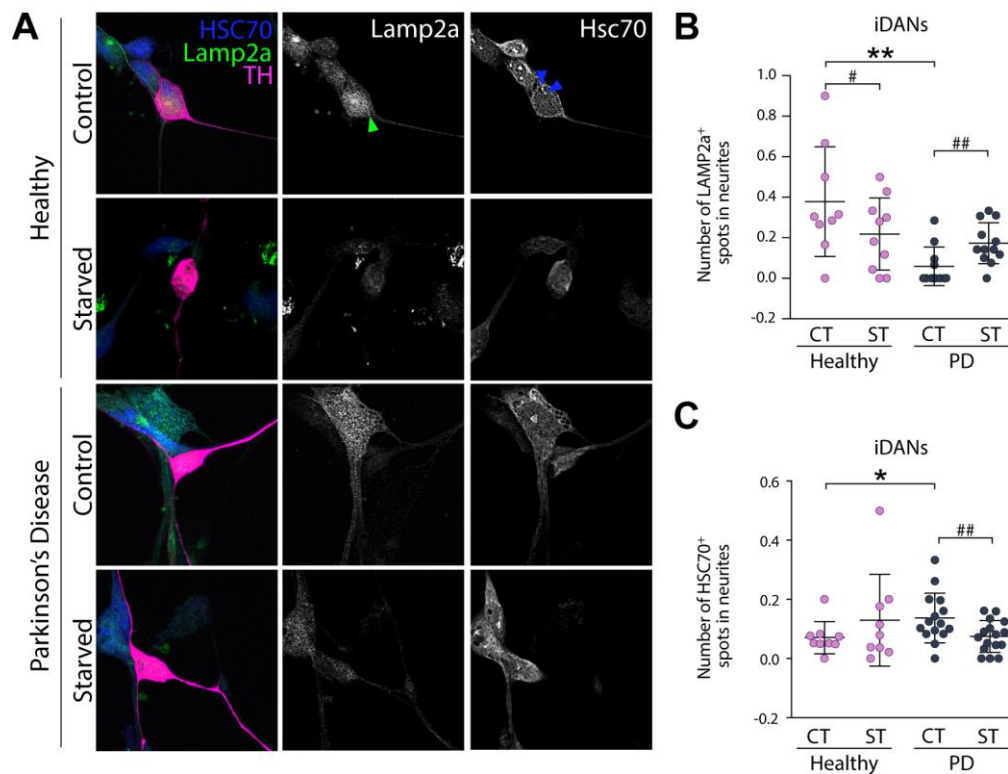


Fig 2. Chaperone-mediated autophagy impairment in PD-iDANs.

(A) LAMP2a-positive dot expression and spot detection analysis of LAMP2a-positive (green arrowhead) and HSC70-positive (blue arrowheads) puncta in TH-positive iDANs.

(B) Quantification of LAMP2a-positive puncta in the neurites of TH-positive iDANs (mean average of 14 TH-positive cells assessed per line, $n=10$ healthy and $n=18$ Parkinson's disease lines). Kruskal-Wallis test, Dunn's multiple comparisons test: $*P=0.0067$; H: Two-tailed paired t-test: $\#P=0.0194$, $df=8$; Parkinson's disease: Wilcoxon matched pairs signed rank test: $\#\#P=0.0098$, $rs=0.339$.

(C) Quantification of HSC70-positive puncta in neurites of TH-positive iDANs (mean average of 95 TH-positive cells assessed per line, $n=8-9$ healthy and $n=16$ Parkinson's disease lines). Mann-Whitney U test: $*P=0.0128$, $U=26.5$. Wilcoxon matched pairs signed rank test: $\#\#P=0.0031$, $rs=0.395$.

Abbreviations: CT: control, H: healthy, PD: Parkinson's disease, ST: starved.

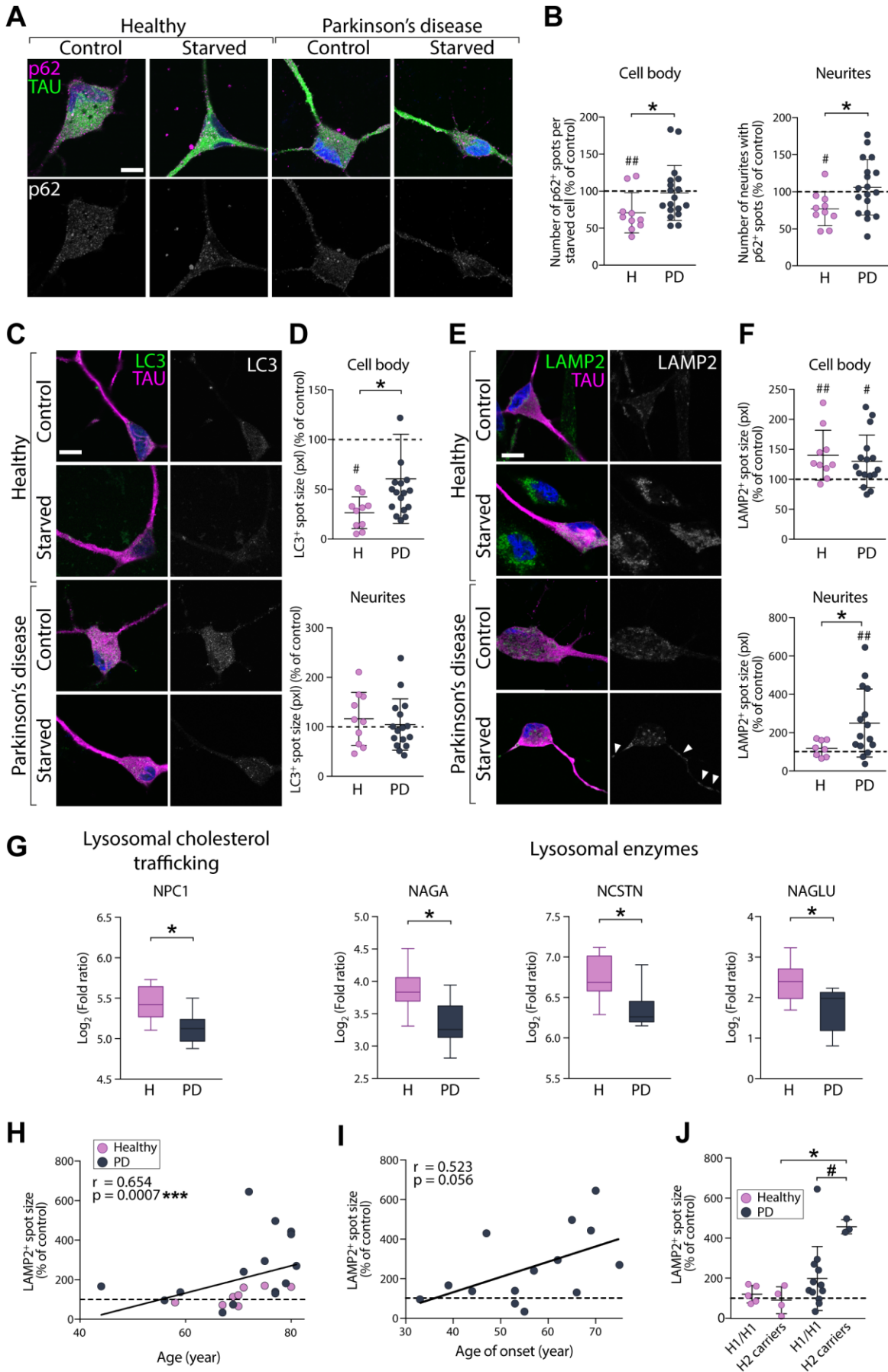


Fig 3. Accumulation of p62, LC3 and LAMP2 in PD-iNs upon starvation.

(A) p62-positive dot expression in TAU-positive iNs. Scale bar = 25 μ m.

(B) Quantification of p62-positive puncta in TAU-positive iNs (mean average of 577 TAU-positive cells assessed per line, n=10 healthy and n=18 Parkinson's disease lines). Cell body: Mann-Whitney test: *P=0.0400, H: two-tailed paired t-test: ##P=0.0056, df=9; Neurite: unpaired t-test: *P=0.0357, df=26, H: two-tailed paired t-test: #P=0.0128, df=9. Data were normalized as % of control condition (not starved).

(C) LC3-positive dot expression in TAU-positive iNs. Scale bar = 10 μ m.

(D) Quantification of LC3-positive puncta in TAU-positive iNs (mean average of 479 TAU-positive cells assessed per line, n=10 healthy and n=18 Parkinson's disease lines). Cell body: two-tailed Mann-Whitney *U* test: *P=0.0311, *U*=51, H: two-tailed paired t-test: ##P=0.0051, df=9. Data were normalized as % of control condition (not starved).

(E) LAMP2-positive dot expression in TAU-positive iNs. Scale bar = 25 μ m

(F) Quantification of LAMP2-positive puncta in TAU-positive iNs (mean average of 202 TAU-positive cells assessed per line, n=10 healthy and n=17 Parkinson's disease lines). Cell body: H: two-tailed paired t-test: ##P=0.0078, df=8, Parkinson's disease: #P=0.0295, df=13. Neurites: Two-tailed unpaired t-test with Welch's correction: *P=0.0136, *U*=24: *P=0.0125, df=18.23, Parkinson's disease: two-tailed paired t-test: ##P=0.0042, df=16.75. Data were normalized as % of control condition (not starved).

(G) Boxplots of log₂ fold changes in expression of genes associated with lysosomal functions (adjusted P value < 0.09, n=10 healthy and n=10 Parkinson's disease lines).

(H) Accumulation of LAMP2-positive puncta upon stress-induced autophagy is associated with the age of the donor (n=23 lines). Spearman's rank correlation: ***P=0.0007; 95% confidence interval: 0.3199 to 0.8437.

(I) association between accumulation of LAMP2-positive puncta upon stress-induced autophagy and the age of onset of Parkinson's disease (n=15 Parkinson's disease lines). Spearman's rank correlation: *P=0.0431; 95% confidence interval: 0.01127 to 0.8263.

(J) More pronounced accumulation of LAMP2-positive puncta upon stress in MAPT H2 carrier Parkinson's disease patients. Kruskal-Wallis test, Dunn's multiple comparisons test: *P=0.0265; two-tailed Mann-Whitney *U* test: #P=0.0250, *U*=3.

Abbreviations: CT: control, H: healthy, PD: Parkinson's disease, ST: starved.

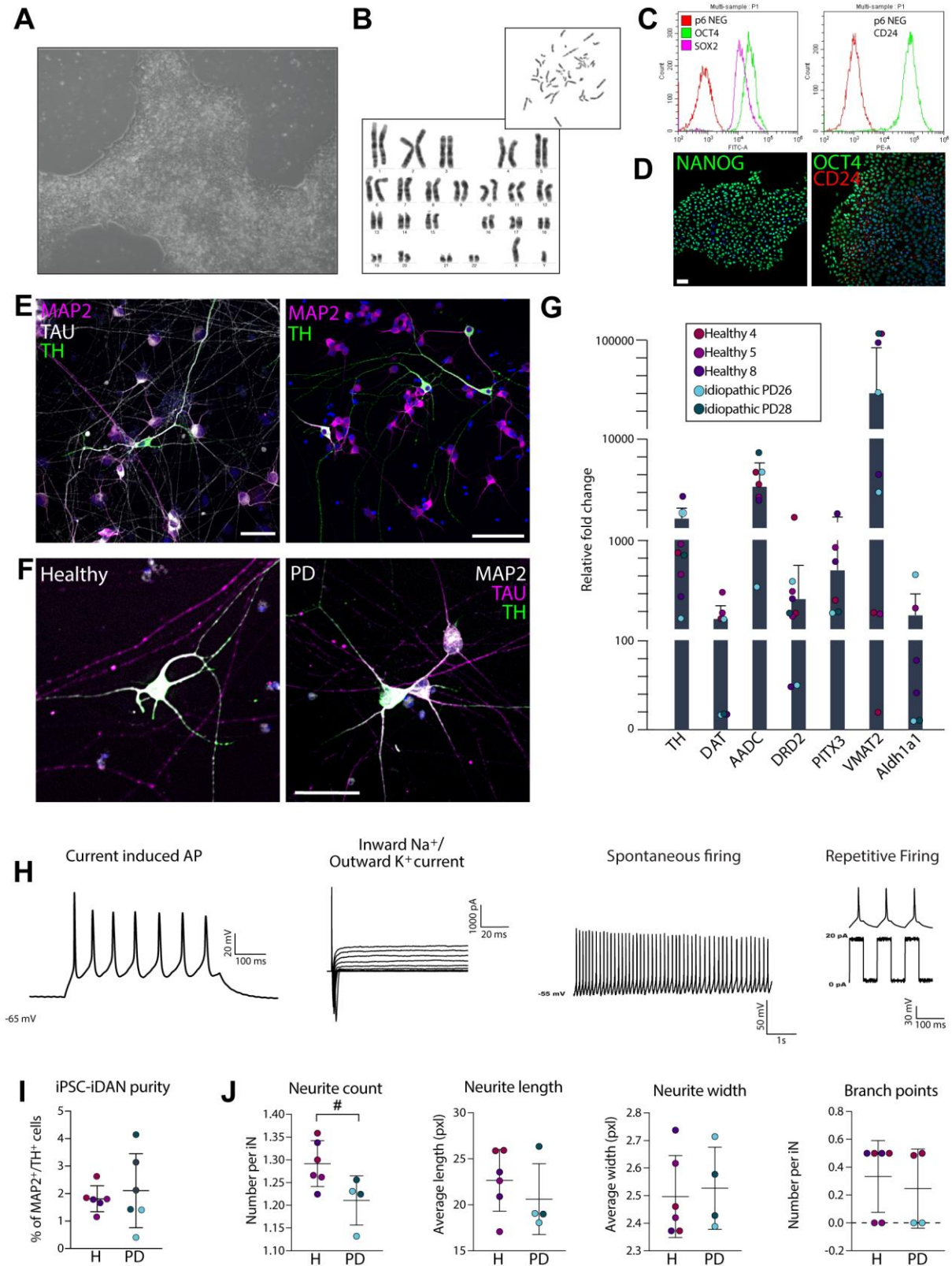
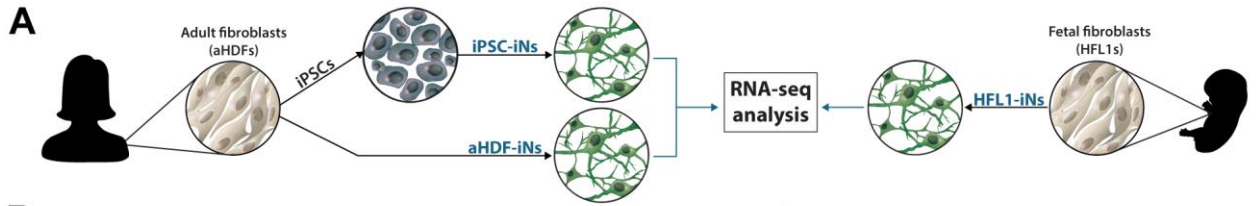


Fig 4. Generation of iDANs from iPSCs of healthy donors and idiopathic PD patients.

(A) Brightfield images of fibroblasts reprogrammed to iPSCs using a StemRNA 3rd Generation Reprogramming kit.

(B) Cells retained a normal karyotype.

- (C) FACS quantification of stem cell markers OCT4, SOX2 and CD24.
- (D) Immunofluorescence staining showing that cells express stem cell markers NANOG, OCT4 and CD24.
- (E) MAP2-positive, TAU-positive and TH-positive iPSC-iDANs. Cells are counterstained with DAPI (in blue). Scale bars = 100µm.
- (F) Representative images of MAP2-positive, TAU-positive and TH-positive iPSC-iDANs derived from healthy donors and PD patients. Cells are counterstained with DAPI (in blue). Scale bars = 25µm.
- (G) Quantitative RT-PCR gene expression quantification of DA genes relative to parental iPSC levels (9 clones from 5 lines). Refer to Table 1 for the information of each donor from which the iPSC cell lines were derived.
- (H) Patch clamp recordings of iDANs reprogrammed from RC17 embryonic stem cells at day 35. ($n = 8$ neurons).
- (I) Quantification of double MAP2-positive and TH-positive cells (from 2 clones; 6 biological replicates).
- (J) Quantification of neurite profile in TAU-positive H-iNs and PD-iNs derived from iPSCs (from 2 clones; 6 biological replicates).



B

| Description | Set size | Enrichment Score | NES | p value | p-adjust |
|--------------------------------------|----------|------------------|--------|---------|----------|
| GO_MULTICELLULAR_ORGANISM_AGING | 28 | -0.627 | -1.872 | 0.003 | 0.015 |
| GO_AGING | 265 | 0.296 | 1.120 | 0.217 | 0.460 |
| GO_NEGATIVE_REGULATION_OF_CELL_AGING | 21 | -0.432 | -1.201 | 0.230 | 0.460 |
| GO_REGULATION_OF_CELL_AGING | 42 | -0.320 | -1.015 | 0.425 | 0.594 |
| GO_POSITIVE_REGULATION_OF_CELL_AGING | 12 | -0.372 | -0.887 | 0.581 | 0.594 |
| GO_CELL_AGING | 96 | -0.249 | -0.935 | 0.594 | 0.594 |

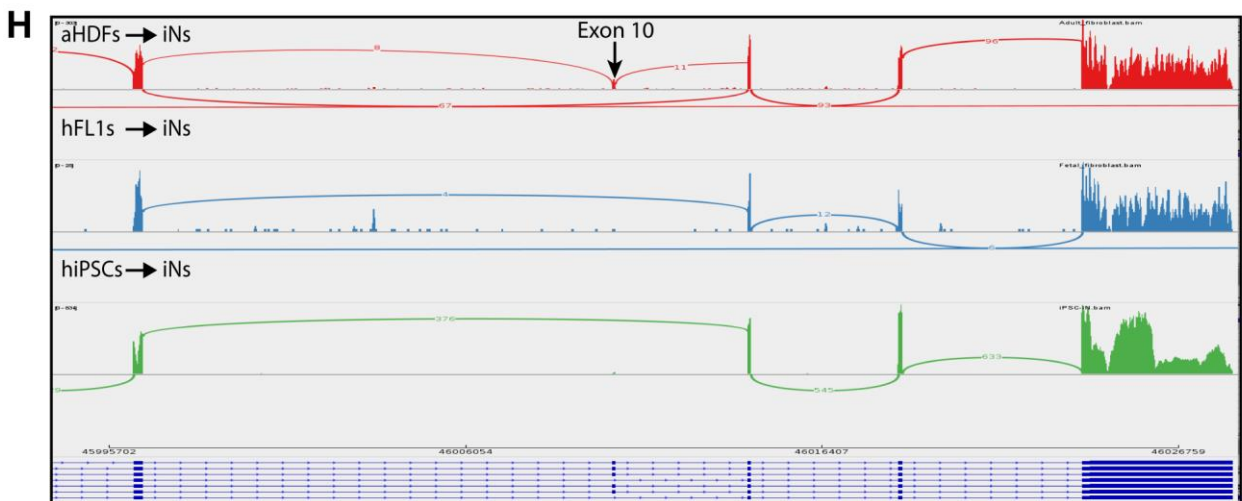
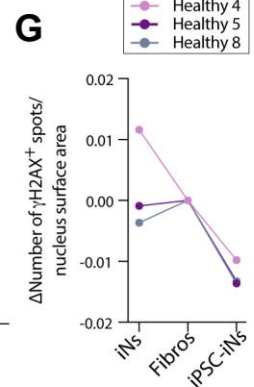
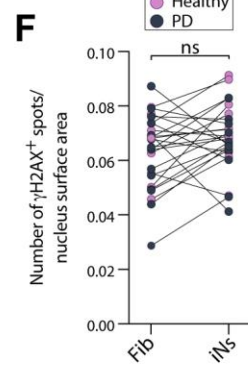
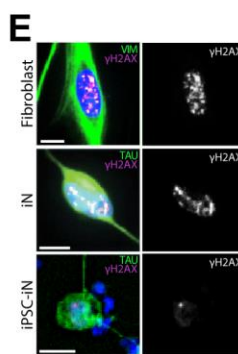
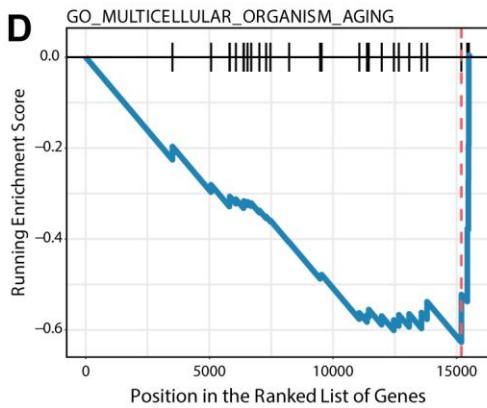
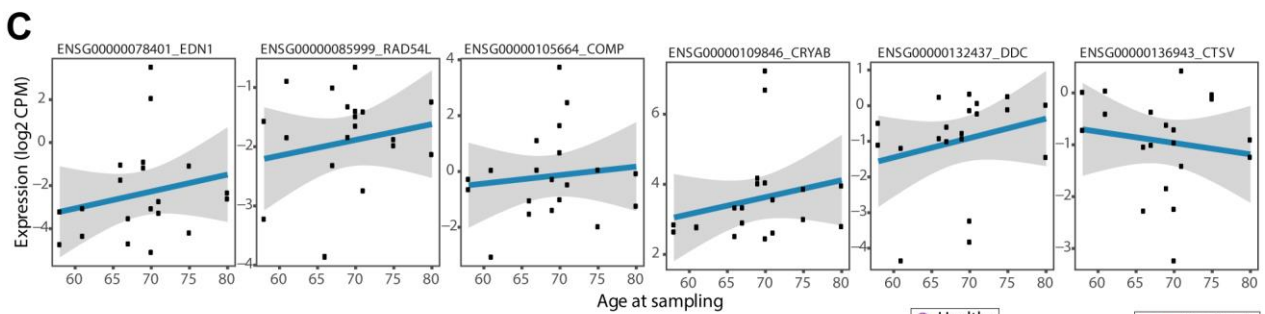


Fig. 5. Assessment of cellular aging.

(A) Overview of RNA-seq experiment.

(B) Gene set enrichment analysis showing enrichment scores of pathways related to cell aging.

(C) After fitting a linear model adjusting for sex and disease status as covariates, genes were ranked based on their association with age at sampling. Top genes showing a clear increase in expression with age were extracted from the gene ontology database and queried against using GSEA (as implemented in the clusterProfiler R package). 5 out of 6 of these gene sets showed negative enrichment scores, indicating association of aging with donor age in this dataset.

(D) “Multicellular organism aging” showing a significant enrichment score.

(E) Representative image of γ H2AX expression in a VIM-positive fibroblast and a TAU-positive iN, both from line #18 (87 years old). Scale bar = 10 μ m.

(F) Quantification of γ H2AX-positive puncta in TAU-positive iNs (mean average of 1,327 fibroblasts and 1,210 TAU-positive cells assessed per line, n=26 lines). Two-tailed paired t-test: P=0.071, df=25.

(G) Quantification of γ H2AX-positive puncta in TAU-positive iNs, parental fibroblasts and iPSC-iNs (mean average of n=329 fibroblasts, n=833 TAU-positive iNs and n=24 iPSC-iNs assessed per line, n=3 lines). Refer to Table 1 for the information of each donor from which the iPSC cell lines were derived.

(H) Sashimi plots visualizing splice junctions and genomic coordinates from merged bam files from adult Fib-iNs (red) and fetal Fib-iNs (blue) indicating that expression of exon 10 (4R isoforms) is only present in iNs from adult fibroblasts. Height of bars indicate expression level and the number on the lines gives number of reads spanning that splice junction.

Abbreviation: ns: not significant, Vim: vimentin.

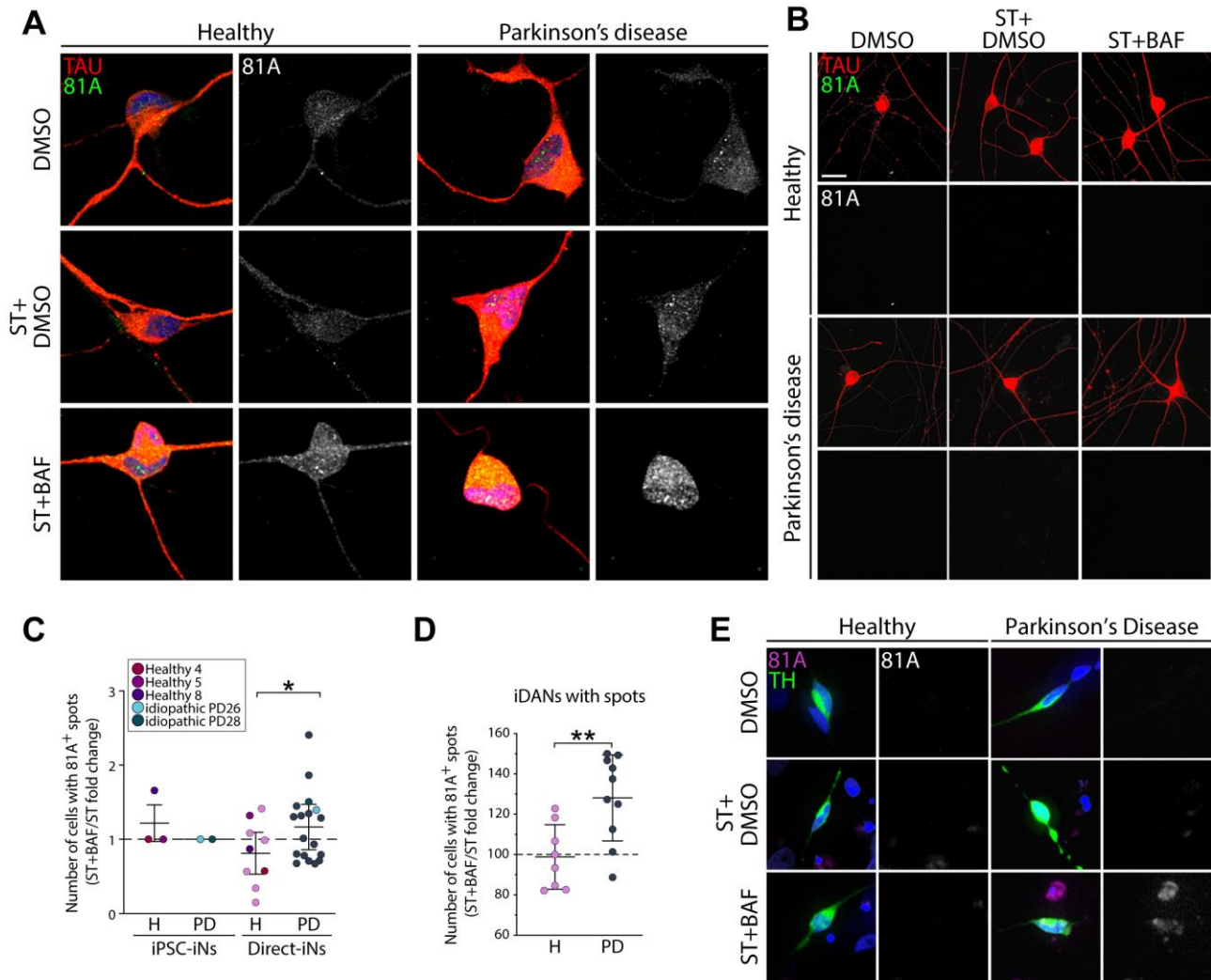


Fig 6. Autophagy impairments lead to an accumulation of phosphorylated α syn in PD-iNs and PD-iDANs.

(A) Confocal images of 81A-positive dot expression in TAU-positive iNs directly reprogrammed from fibroblasts.

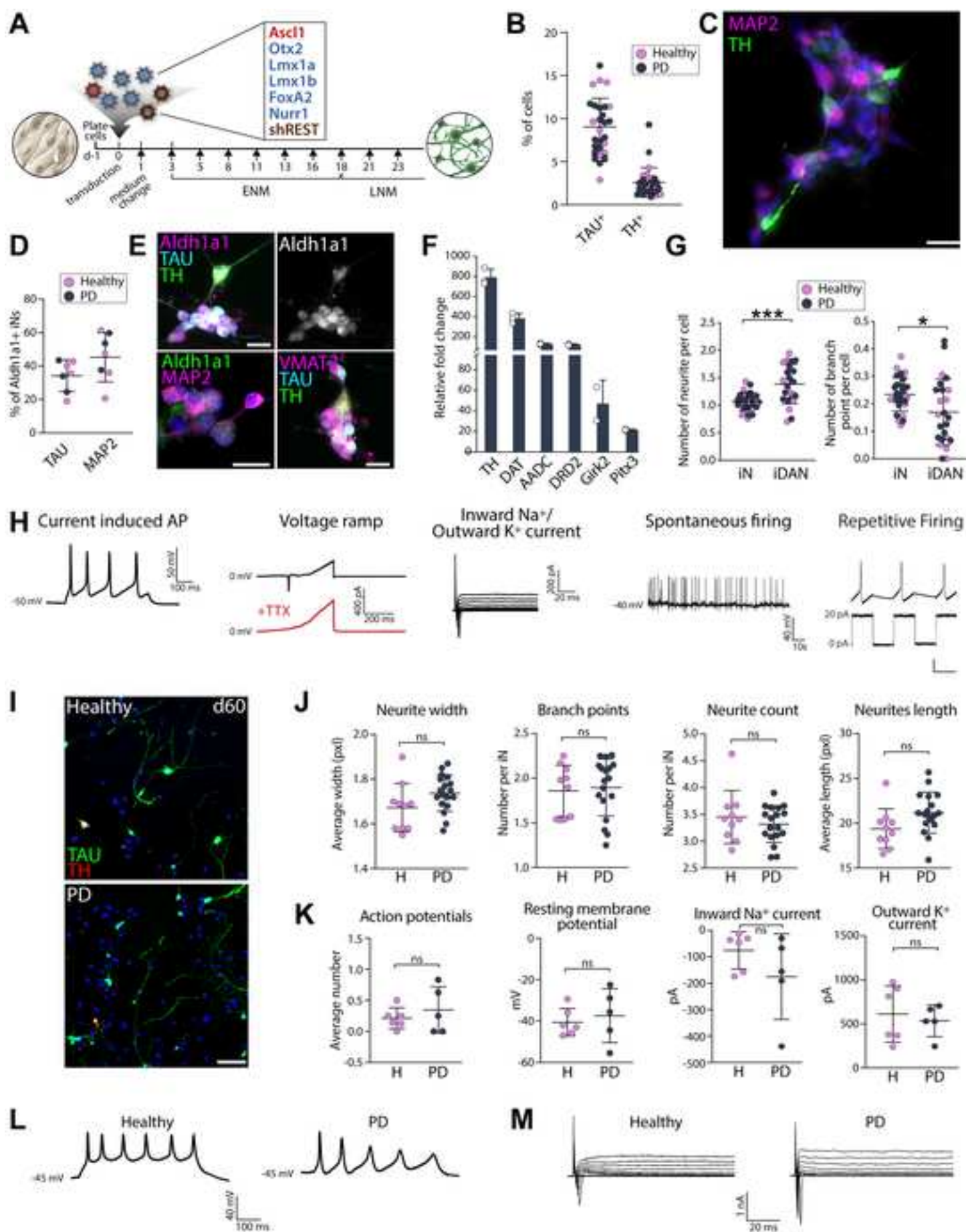
(B) Fluorescent images of 81A-positive dot expression in TAU-positive iNs reprogrammed from iPSCs.

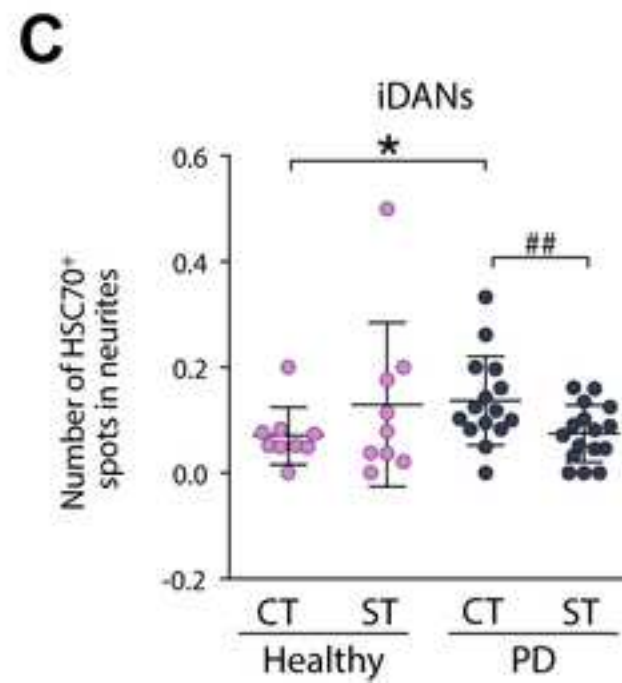
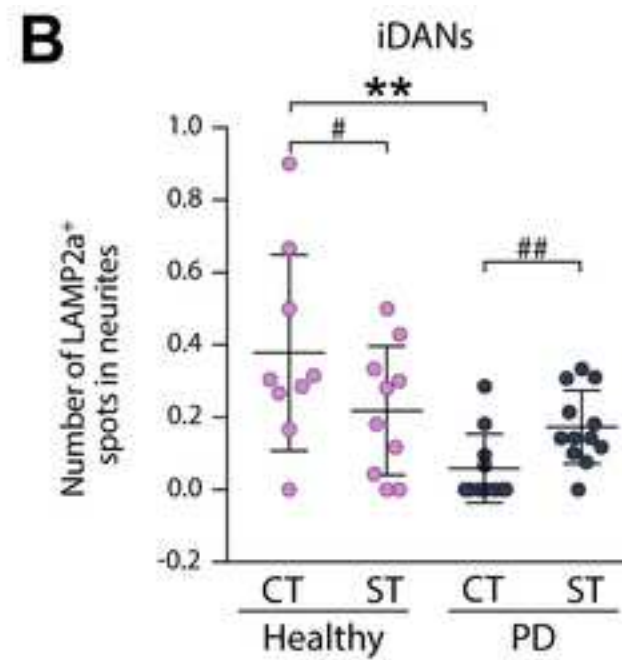
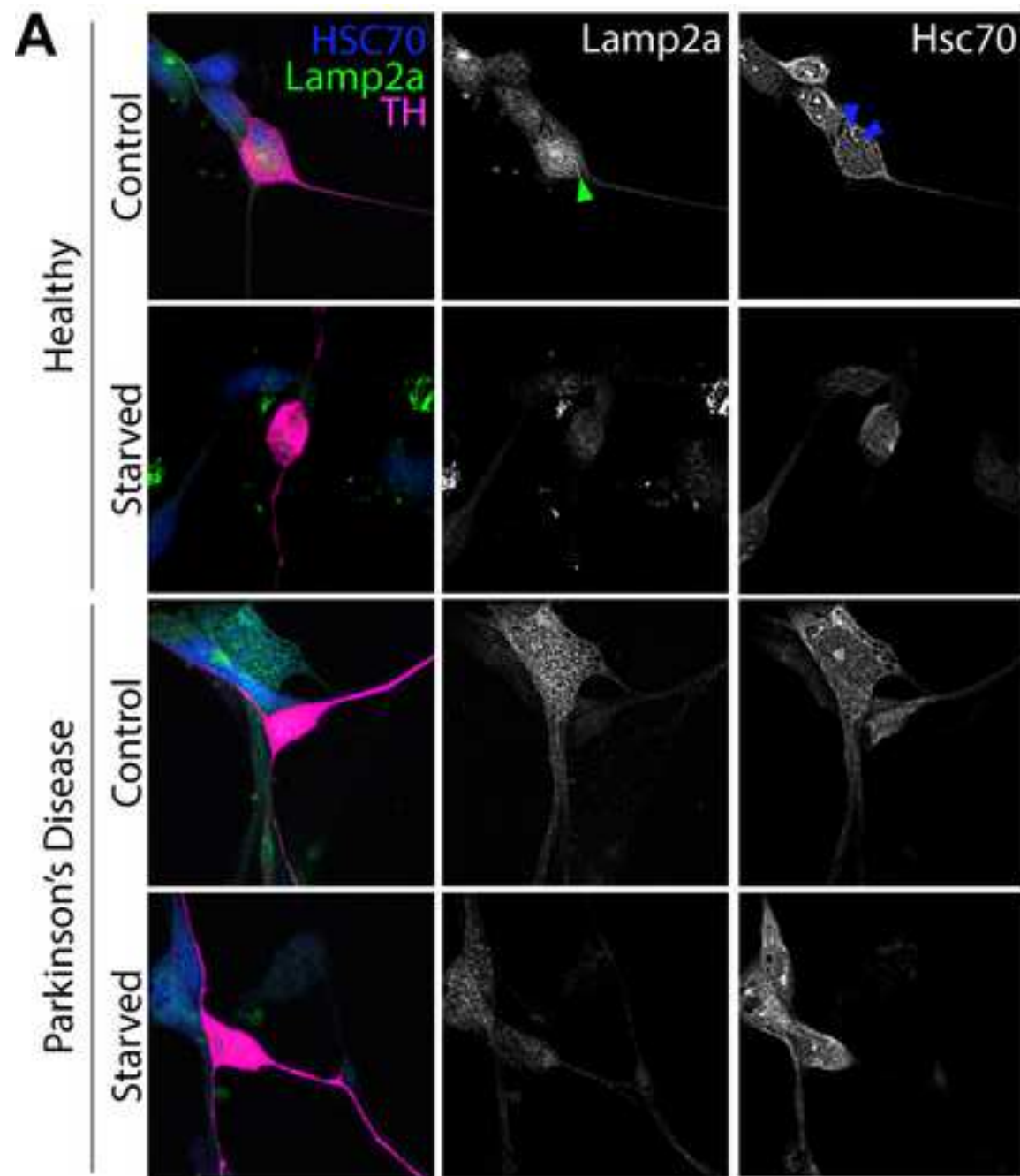
(C) Quantification of TAU-positive iNs with 81A-positive (α syn pSer129) puncta in the cell body (iPSCs-iNs: mean average of 180 TAU-positive cells assessed per line, $n=3$ healthy and $n=2$ PD lines; Direct-iNs: mean average of 1,461 TAU-positive cells assessed per line, $n=9$ healthy and $n=18$ PD lines). Two-tailed unpaired t-test: $*P=0.0329$, $df=25$. Refer to Table 1 for the information of each donor from which the iPSC cell lines were derived.

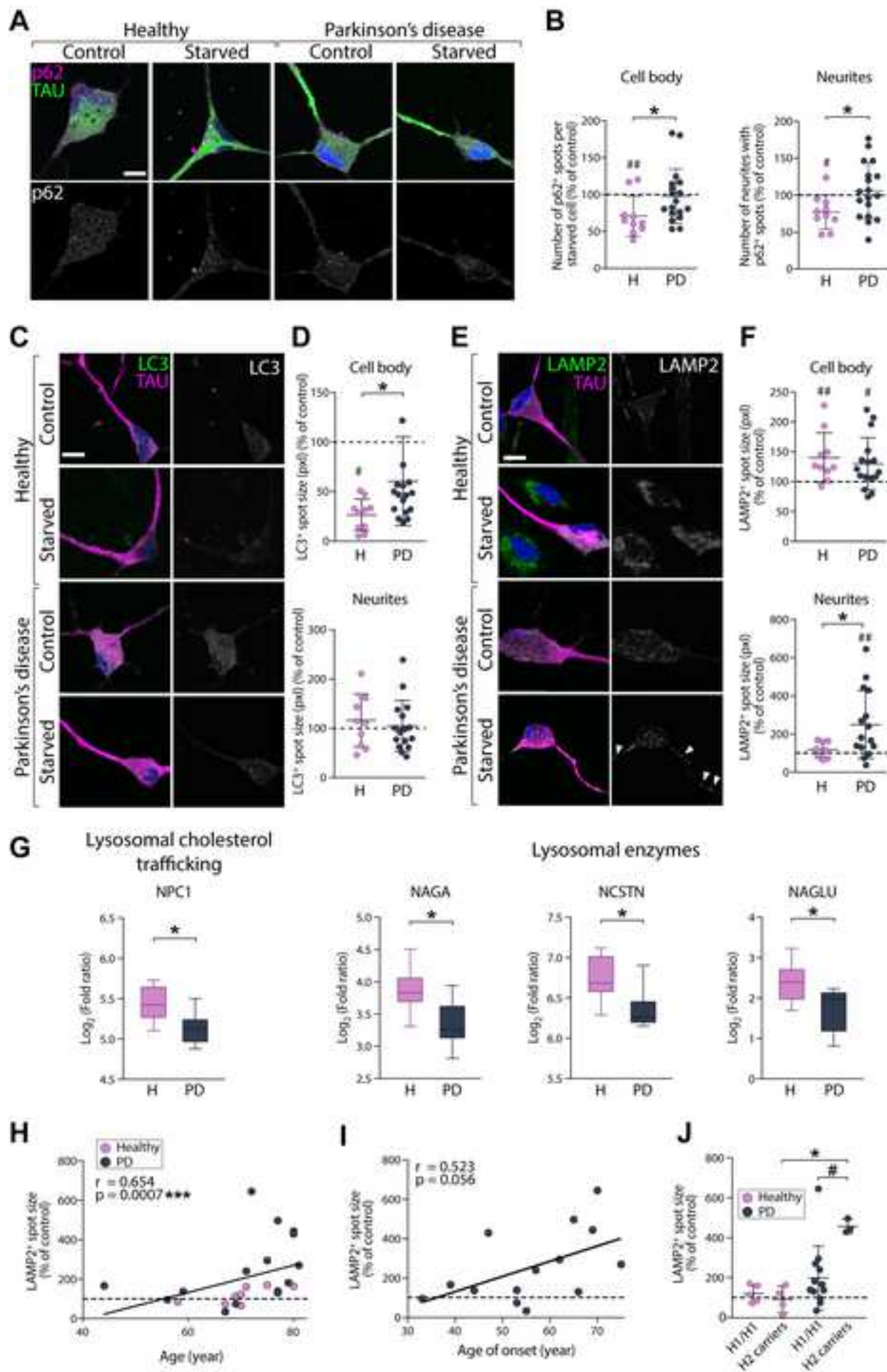
(D) Quantification of TAU-positive/TH-positive iDANs with 81A-positive puncta in the cell body (mean average of 28 TAU-positive/TH-positive cells assessed per line, $n=8$ healthy and $n=10$ PD lines). Two-tailed unpaired t-test: $**P=0.0054$, $df=16$.

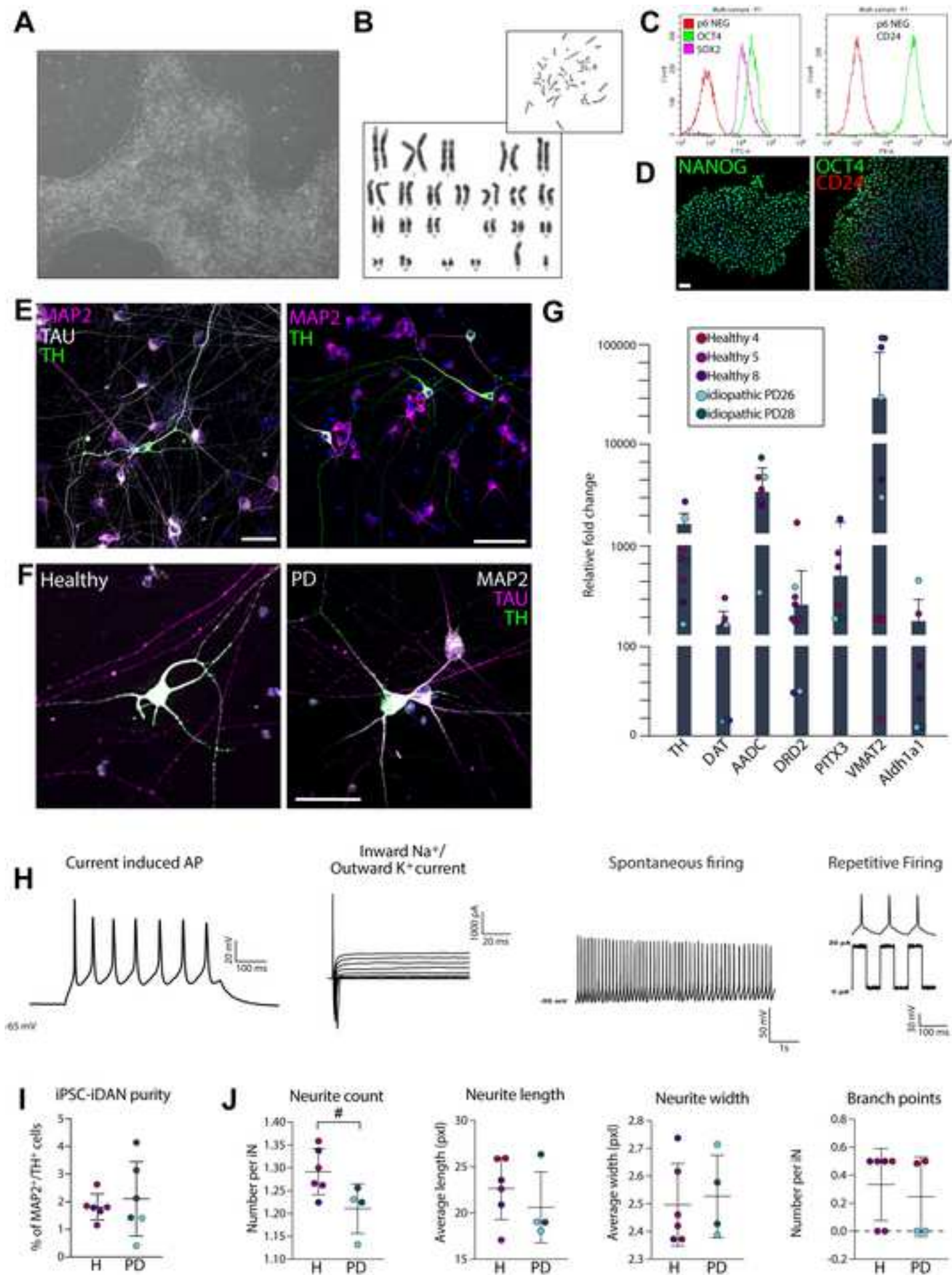
(E) 81A-positive dot expression (in magenta) in TH-positive iDANs (in green) directly reprogrammed from fibroblasts.

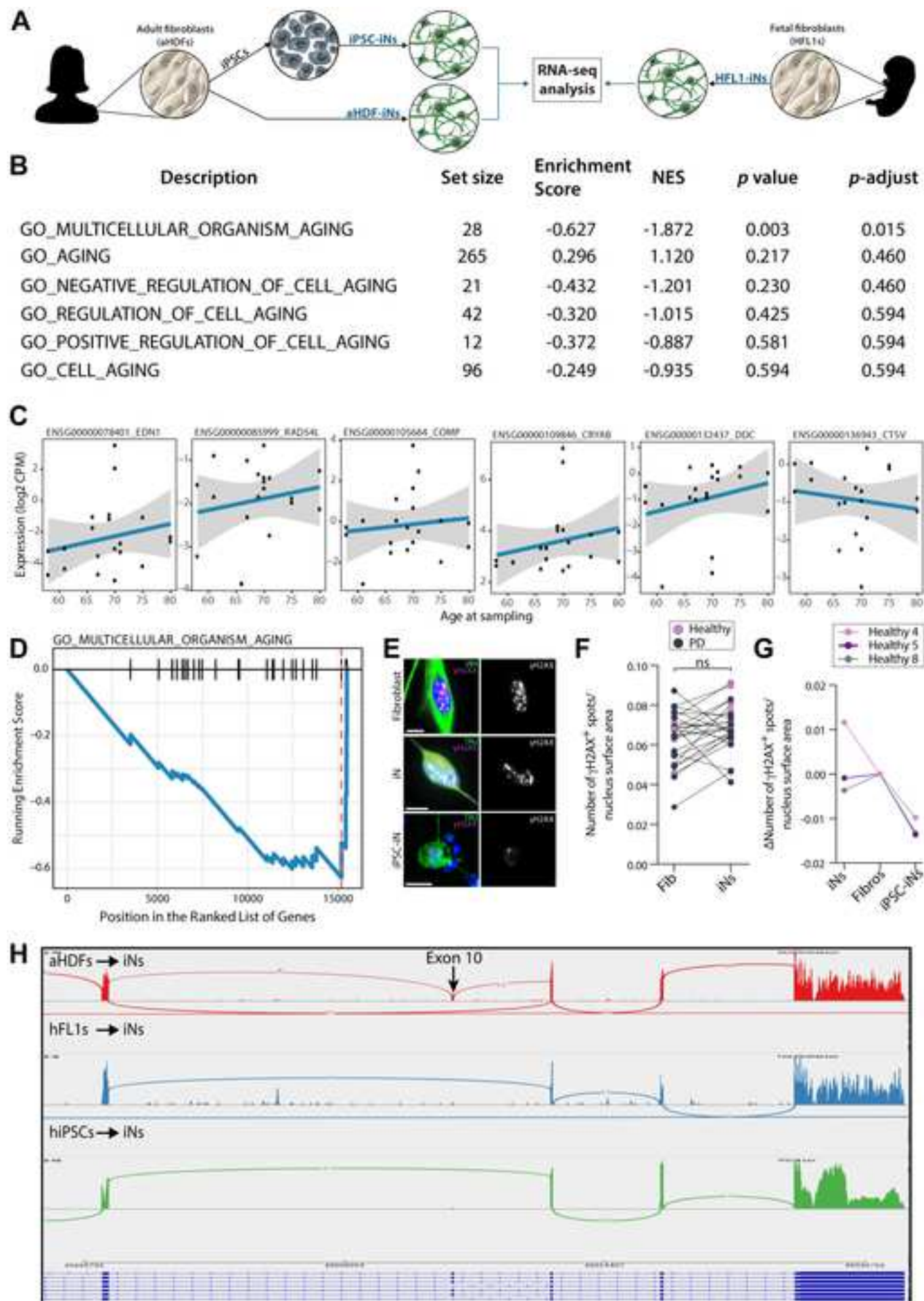
Abbreviations: BAF: Bafilomycin A1, H: healthy; PD: Parkinson's disease, ST: starved.

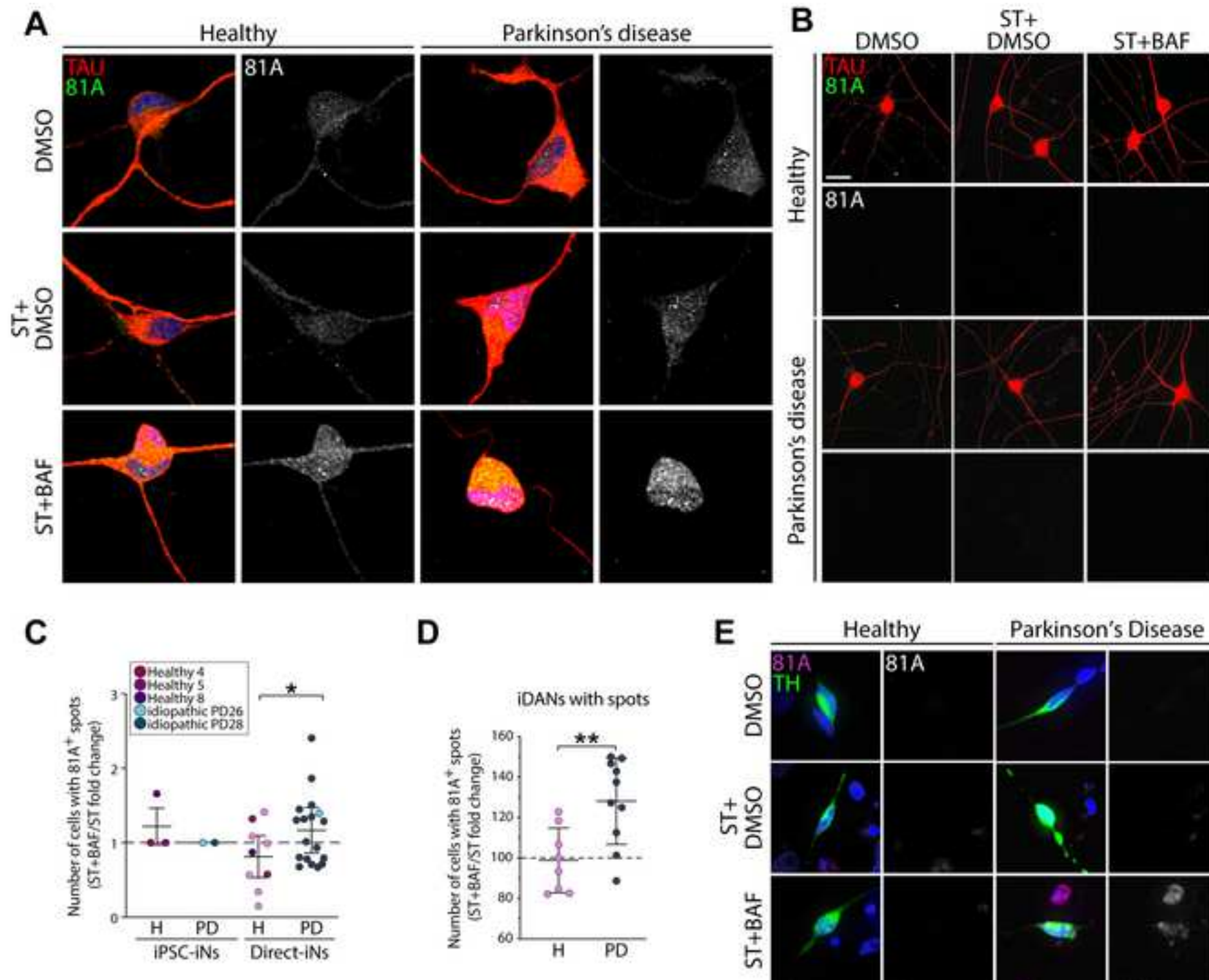












Supplemental figures

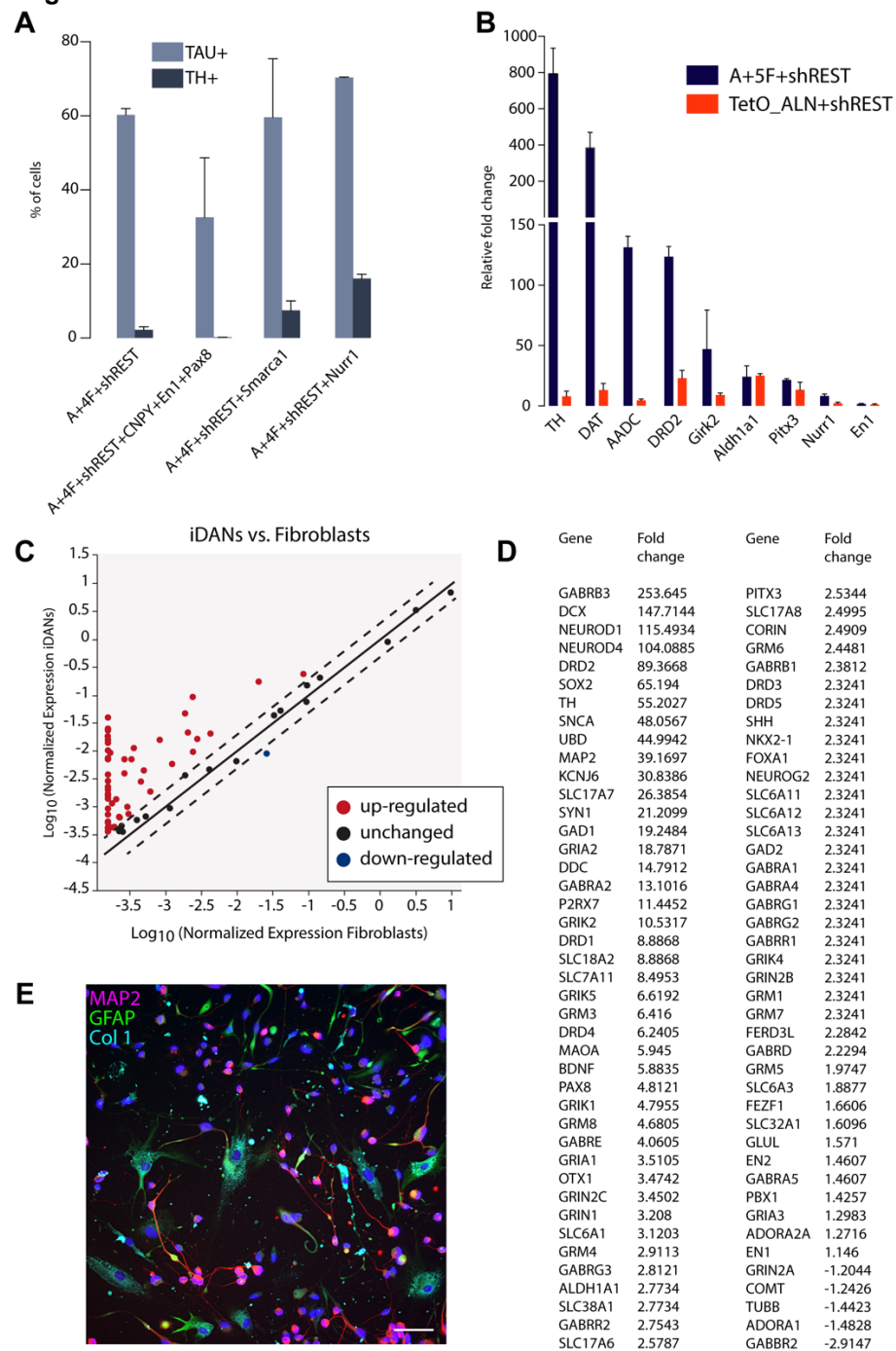


Figure S1 related to Figure 1. Generation of iDANs.

(A) Quantification of TAU-positive and TH-positive cells using different reprogramming factors. A: Ascl1, 4F: Lmx1a, Lmx1b, FoxA2, Otx2.

(B) Gene expression quantification of DA genes relative to parental fibroblast levels (from 2 to 3 biological replicates). 5F: Lmx1a, Lmx1b, FoxA2, Otx2, Nurr1. TetO_ALN: Ascl1, Lmx1a, Nurr1 from (Caiazza et al., 2011).

(C) Fold change of all the neuronal and dopaminergic related genes on the qPCR array as compared to parental fibroblasts. Significantly up- and down-regulated genes are in red and blue, respectively.

(D) Fold change of the top up-regulated neuronal, dopaminergic, glutamatergic and GABAergic related genes as compared to parental fibroblasts.

(E) MAP2, GFAP and Collagen 1 expression at 25 days following the start of conversion with the pB.pA.shREST all-in-one vector. Scale bar = 100 μ m.

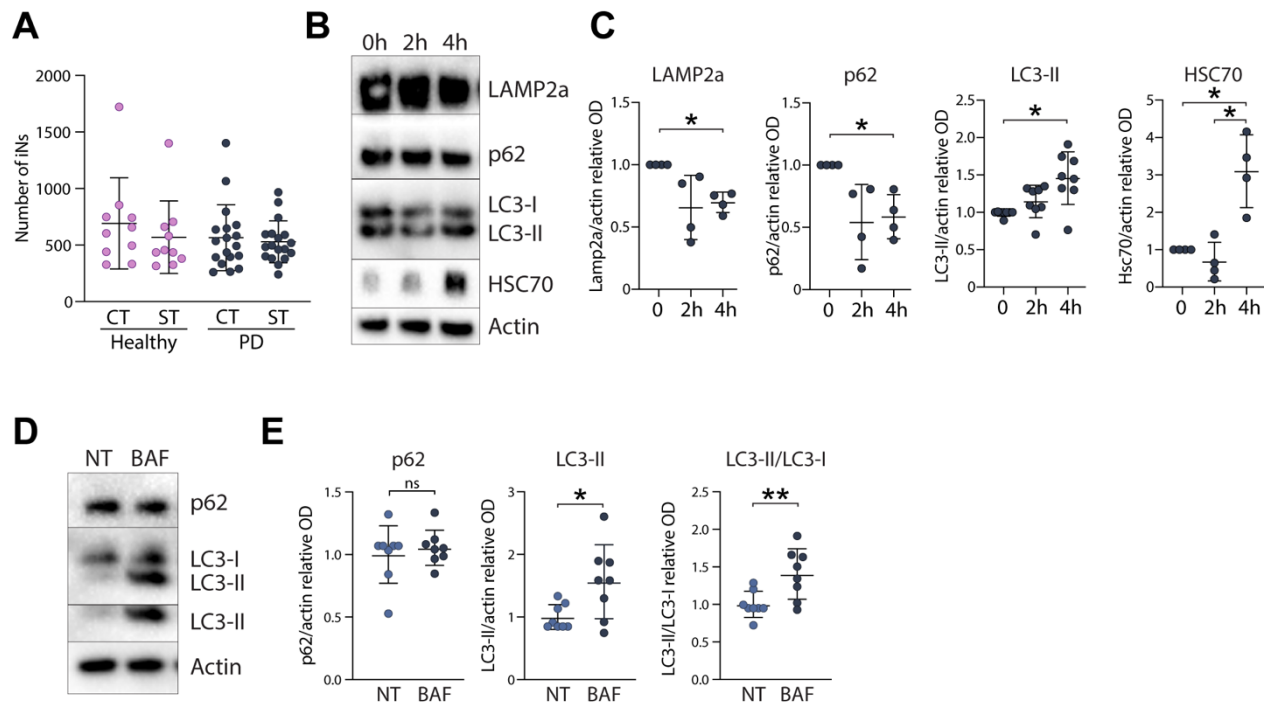


Figure S2. Validation of starvation and Bafilomycin regimen in iNs.

(A) Quantification of the number of TAU+ iNs following a 4-hour starvation period.

(B) Representative WB image showing LAMP2a, SQSTM1 (p62), LC3, HSC70 and Actin immunolabeling in iNs from a healthy donor starved for 0, 2 and 4 hours.

(C) OD quantification of LAMP2a, SQSTM1 (p62), LC3, HSC70 immunoblots in iNs starved for 0, 2 and 4 hours. One-way ANOVA on repeated measures, Tukey post-hoc: * $p < 0.05$. Data are shown as mean \pm SD. Values were normalized to non-treated expression levels and corrected to actin values.

(D) Representative WB image showing SQSTM1 (p62), LC3 and Actin immunolabeling in non-treated (NT) and Bafilomycin A1 (BAF) treated healthy donor iNs.

(E) OD quantification of p62, LC3 immunoblots in NT and BAF treated healthy donor iNs. Two-tailed unpaired t-test: * $P < 0.05$; ** $P < 0.01$. Data are shown as mean \pm SD. Values were normalized to non-treated expression levels and corrected to actin values.

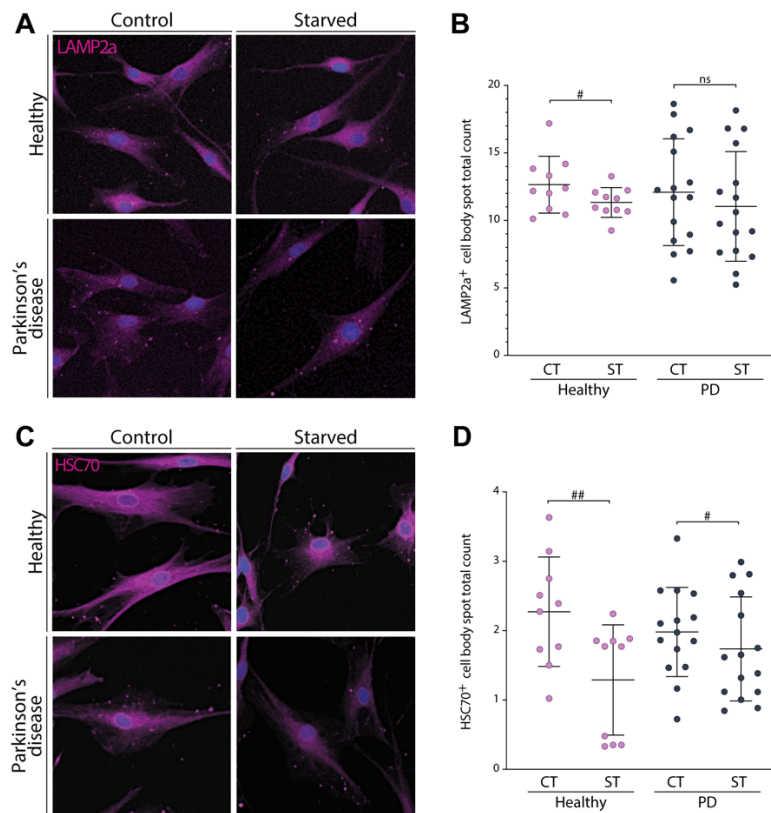


Figure S3 related to Figure 2. No accumulation of LAMP2a and HSC70 in PD-fibroblasts upon starvation.

(A) LAMP2a-positive dot expression in fibroblasts.

(B) Quantification of LAMP2a-positive dots in fibroblasts (mean average of 2,949 cells assessed per line). One-way ANOVA, Bonferroni post-hoc: $P=0.59$. Paired student's t-test: $\#P<0.05$, as compared to the non-starved condition.

(C) HSC70-positive dot expression and spot detection analysis in fibroblasts.

(D) Quantification of HSC70-positive dots in fibroblasts (mean average of 2,949 cells assessed per line). Kruskal-Wallis test, Dunn's multiple comparisons test: $P=0.11$; H: Wilcoxon matched pairs signed rank test: $##P=0.0098$, $r_s=0.346$. PD: Two-tailed paired t-test: $\#P=0.0406$, $df=13$.

Abbreviations: CT: control, H: healthy, ns: not significant, PD: Parkinson's disease, ST: starved.

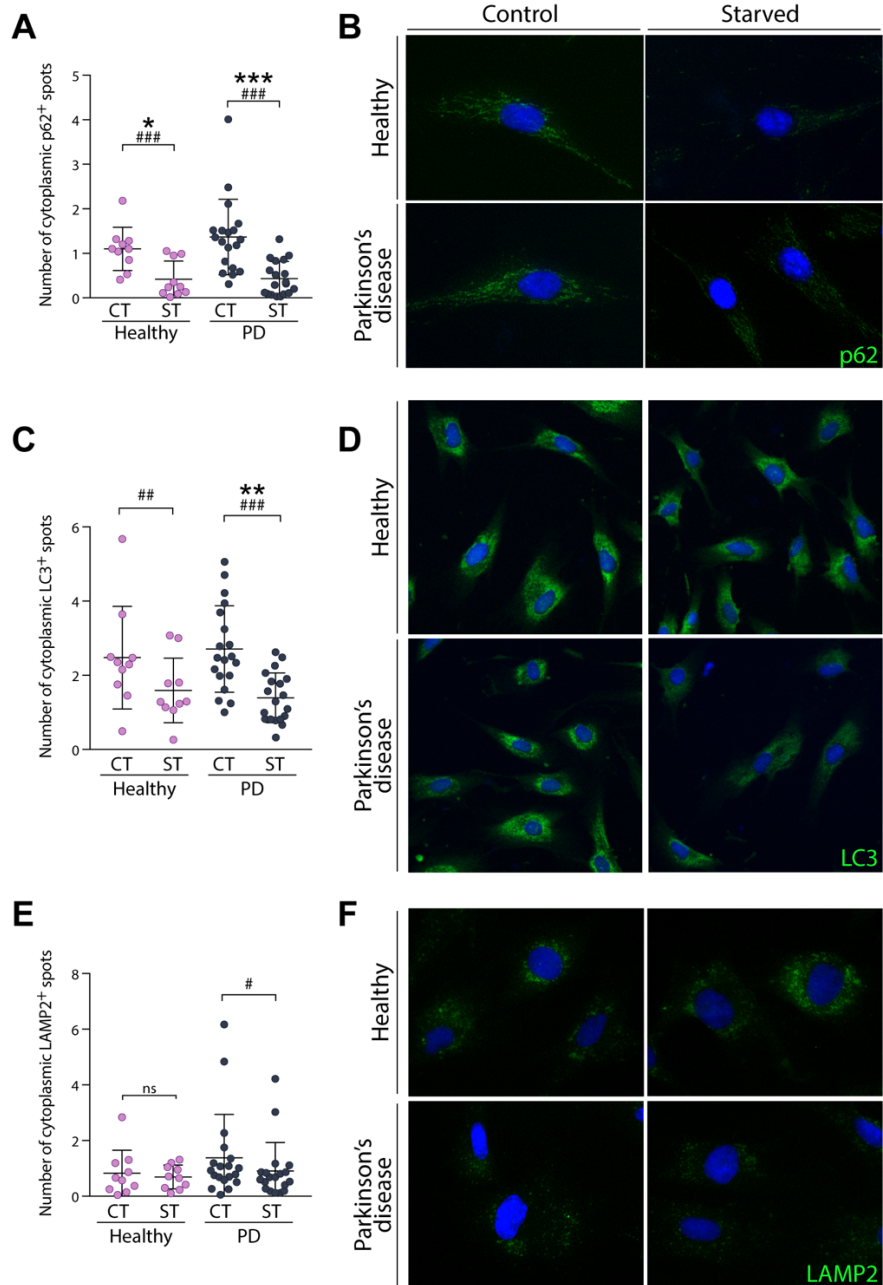


Figure S5 related to Figure 3. No accumulation of p62, LC3 and LAMP2 in PD-fibroblasts upon starvation.

(A) p62-positive dot expression and spot detection analysis in fibroblasts.

(B) Quantification of p62-positive dots in fibroblasts (mean average of 625 cells assessed per line). One-way ANOVA, Bonferroni post-hoc: * $p < 0.05$, *** $p < 0.001$. Paired student's t-test: ### $p < 0.001$ as compared to the condition without starvation.

(C) LC3-positive dot expression and spot detection analysis in fibroblasts.

(D) Quantification of LC3-positive dots in fibroblasts (mean average of 651 cells assessed per line). One-way ANOVA, Bonferroni post-hoc: ** $p < 0.01$, as compared to the healthy group. Paired student's t-test: ## $p < 0.01$, ### $p < 0.001$ as compared to the condition without starvation.

(E) LAMP2-positive dot expression and spot detection analysis in fibroblasts.

(F) Quantification of LAMP2-positive dots in fibroblasts (mean average of 1,126 cells assessed per line). Paired student's t-test: # $p < 0.05$ as compared to the condition without starvation. Abbreviations: CT: control, H: healthy, ns: not significant, PD: Parkinson's disease, ST: starved.

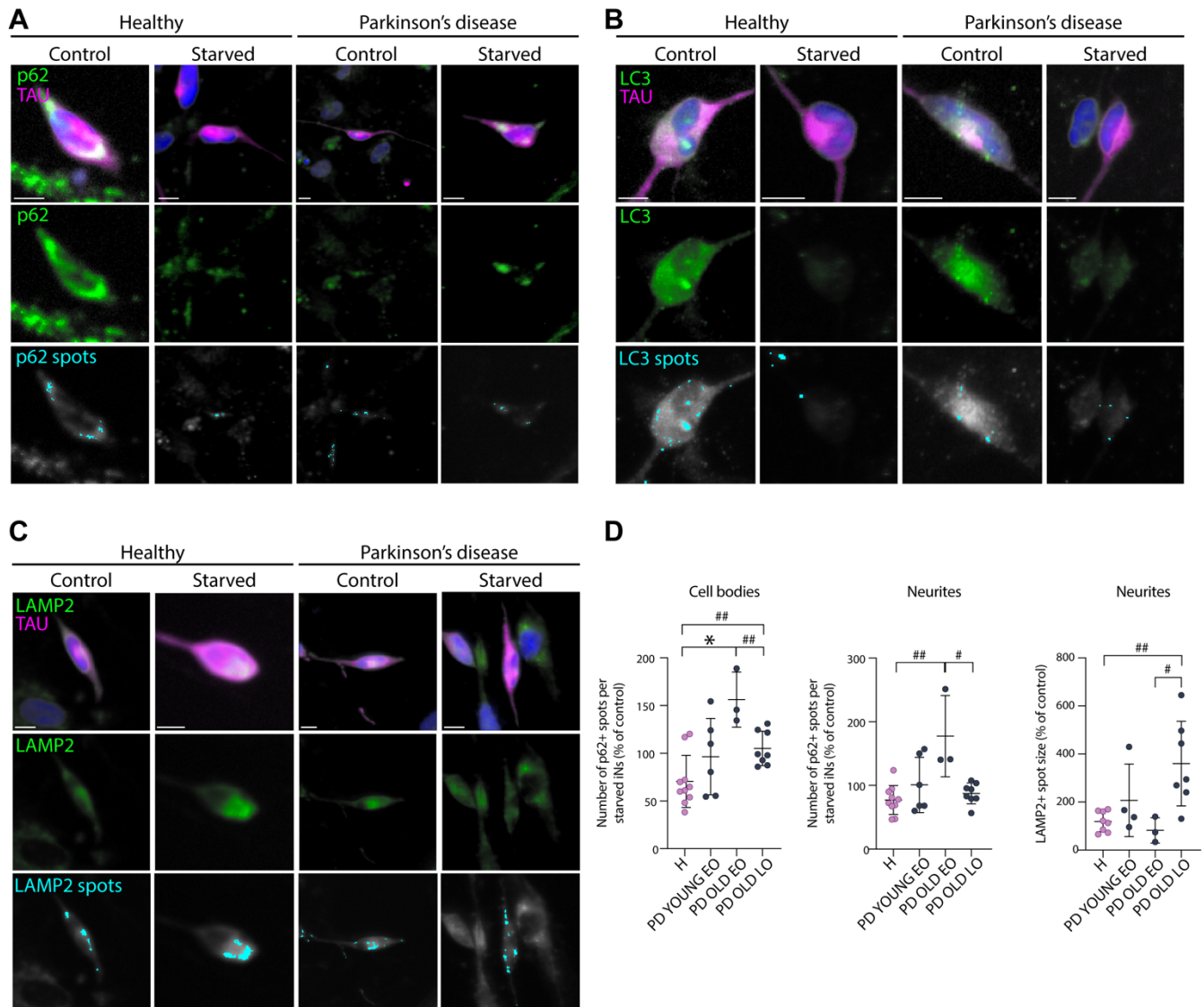


Figure S6 related to Figure 3. p62, LC3 and LAMP2 expression in iNs vs. iDANs upon starvation.

(A) p62-positive dot expression in TAU-positive cells. Cyan overlays represent the puncta that were quantified for analysis.

(B) LC3-positive dot expression in TAU-positive cells. Cyan overlays represents the puncta that were quantified for analysis.

(C) LAMP2-positive dot expression in TAU-positive cells. Cyan overlays represent the puncta that were quantified for analysis.

(D) Differences in the number of p62-positive dots per starved iNs in different cell compartments, and of LAMP2+ spot size per neurite depending on the age and age at onset of the PD patient. Young EO: patients younger than 60 years of age, with disease onset before 60 years of age. Old EO: patients older than 60 years of age, with disease onset before 60 years of age. Old LO: patients older than 60 years of age, with disease onset after 60 years of age. Kruskal-Wallis test: * $P=0.0106$; Unpaired t-test or Mann-Whitney test (depending on the normality of the distribution): # $P<0.05$, ## $P<0.01$.

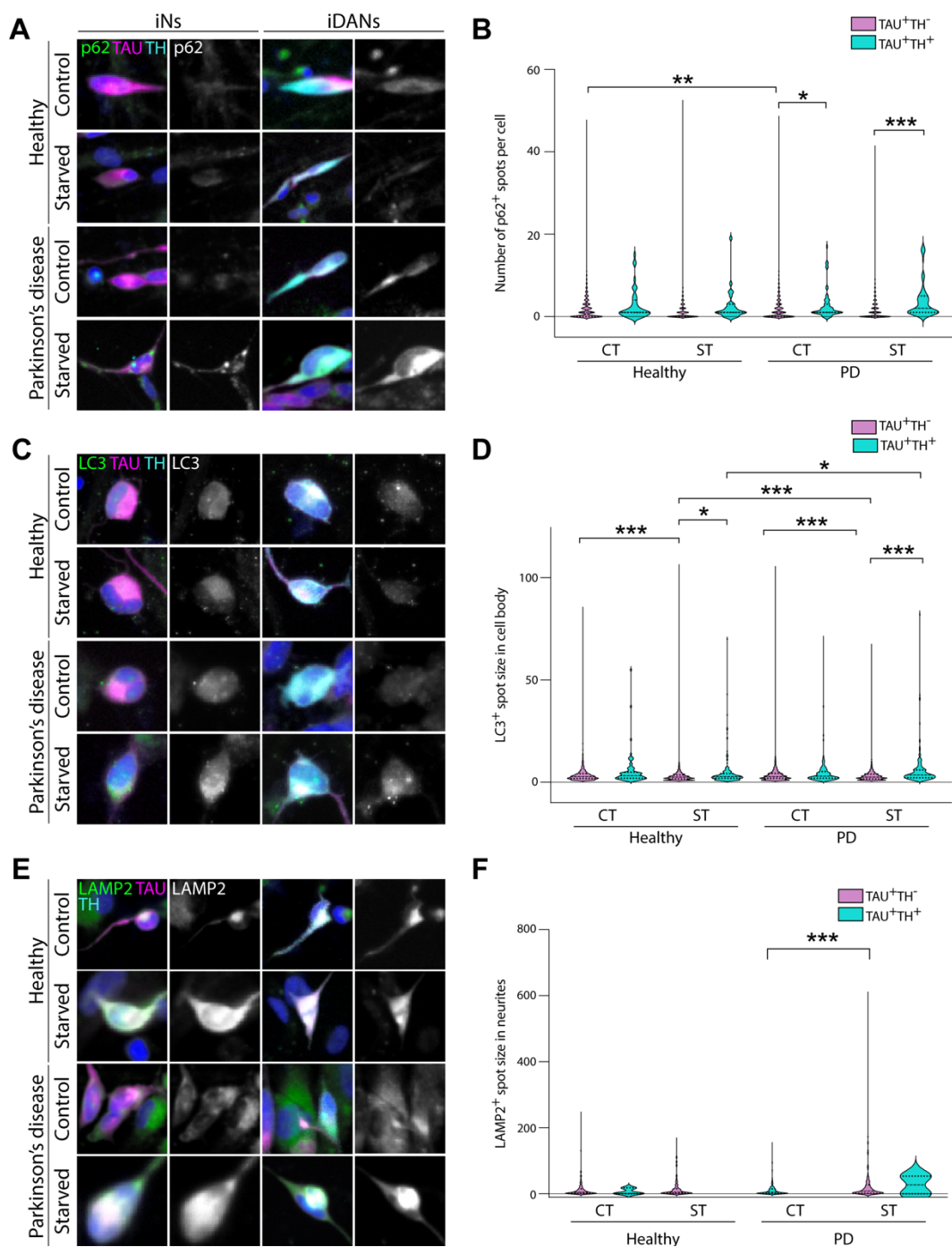


Figure S7 related to Figure 3. p62, LC3 and LAMP2 in iNs vs. iDANs upon starvation.

(A) p62-positive dot expression in TAU-positive/TH-negative and TAU-positive/TH-positive cells.

(B) Violin plot showing quantification of p62-positive dots in TAU-positive/TH-negative and TAU-positive/TH-positive cells. Kruskal-Wallis test, Dunn's multiple comparisons test: * $p < 0.05$, ** $p < 0.01$, *** $p < 0.001$.

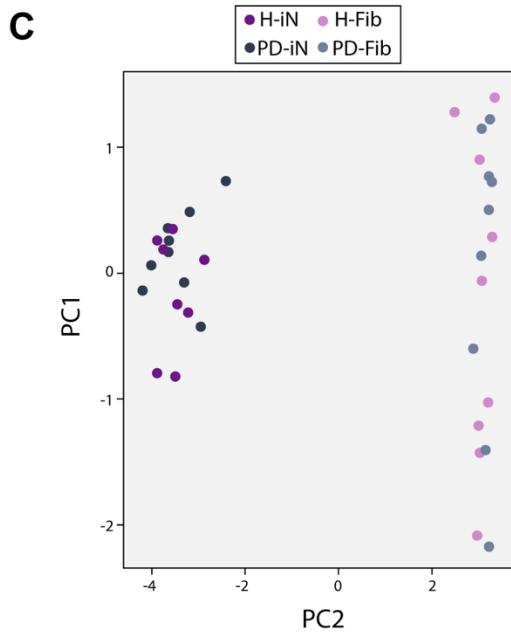
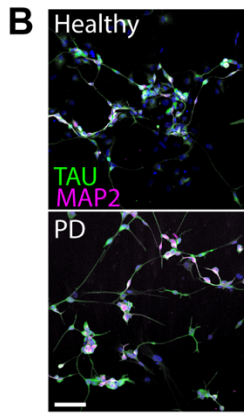
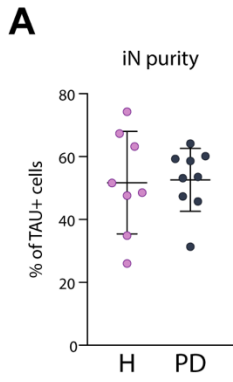
(C) LC3-positive dot expression in TAU-positive/TH-negative and TAU-positive/TH-positive cells.

(D) Violin plot showing quantification of LC3-positive dots in TAU-positive/TH-negative and TAU-positive/TH-positive cells. Kruskal-Wallis test, Dunn's multiple comparisons test: * $p < 0.05$, *** $p < 0.001$.

(E) LAMP2-positive dot expression in TAU-positive/TH-negative and TAU-positive/TH-positive cells.

(F) Violin plot showing quantification of LAMP2-positive dots in TAU-positive/TH-negative and TAU-positive/TH-positive cells. Kruskal-Wallis test, Dunn's multiple comparisons test: *** $p < 0.001$.

Abbreviations: CT: control, H: healthy, PD: Parkinson's disease, ST: starved.



D

| Pathway | Source | Qvalue | Genes |
|---|---------------------------------------|-----------|-------|
| CELL CYCLE, MITOTIC | REACTOME DATABASE ID RELEASE 59 | 0.0000000 | 430 |
| M PHASE | REACTOME | 0.0000000 | 242 |
| HALLMARK_G2M_CHECKPOINT | MSIGDB_C2 | 0.0000000 | 191 |
| HALLMARK_E2F_TARGETS | MSIGDB_C2 | 0.0000000 | 193 |
| MITOTIC PROMETAPHASE | REACTOME | 0.0000000 | 101 |
| NEURONAL SYSTEM | REACTOME | 0.0000249 | 225 |
| TRANSMISSION ACROSS CHEMICAL SYNAPSES | REACTOME | 0.0037818 | 146 |
| NEUROTRANSMITTER RECEPTOR BINDING AND DOWNSTREAM TRANSMISSION IN THE POSTSYNAPTIC CELL | REACTOME | 0.0564830 | 97 |

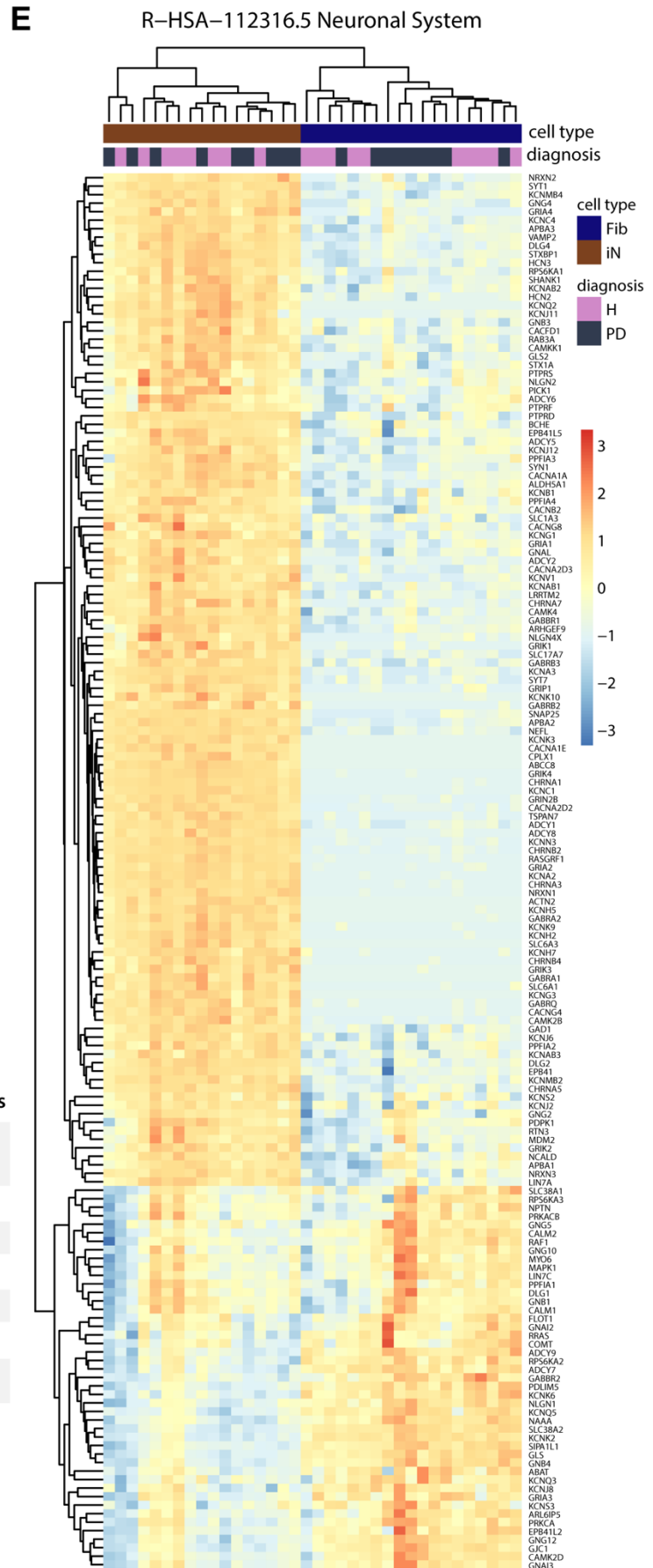


Figure S8. iN transcription profile.

(A) Quantification of the TAU-positive cell purity from a biological replicate of the cells sent for RNA-seq (mean average of 16,221 cells assessed per line).

(B) Double TAU-positive and MAP2-positive iNs from a biological replicate of the cells sent for RNA-seq. Scale bar = 100 μ m.

(C) Principal component analysis showing a separation of the reprogrammed iNs from the parental fibroblasts on PC2.

(D) Gene set enrichment analysis showing top ten most up and down regulated pathways in iNs compared to fibroblasts.

(E) Hierarchical clustering of RNA-seq samples, using Euclidean distance on normalized and log2-transformed read counts.

Abbreviations: Fib: fibroblasts; H: healthy, iN: induced neurons; PD: Parkinson's disease.

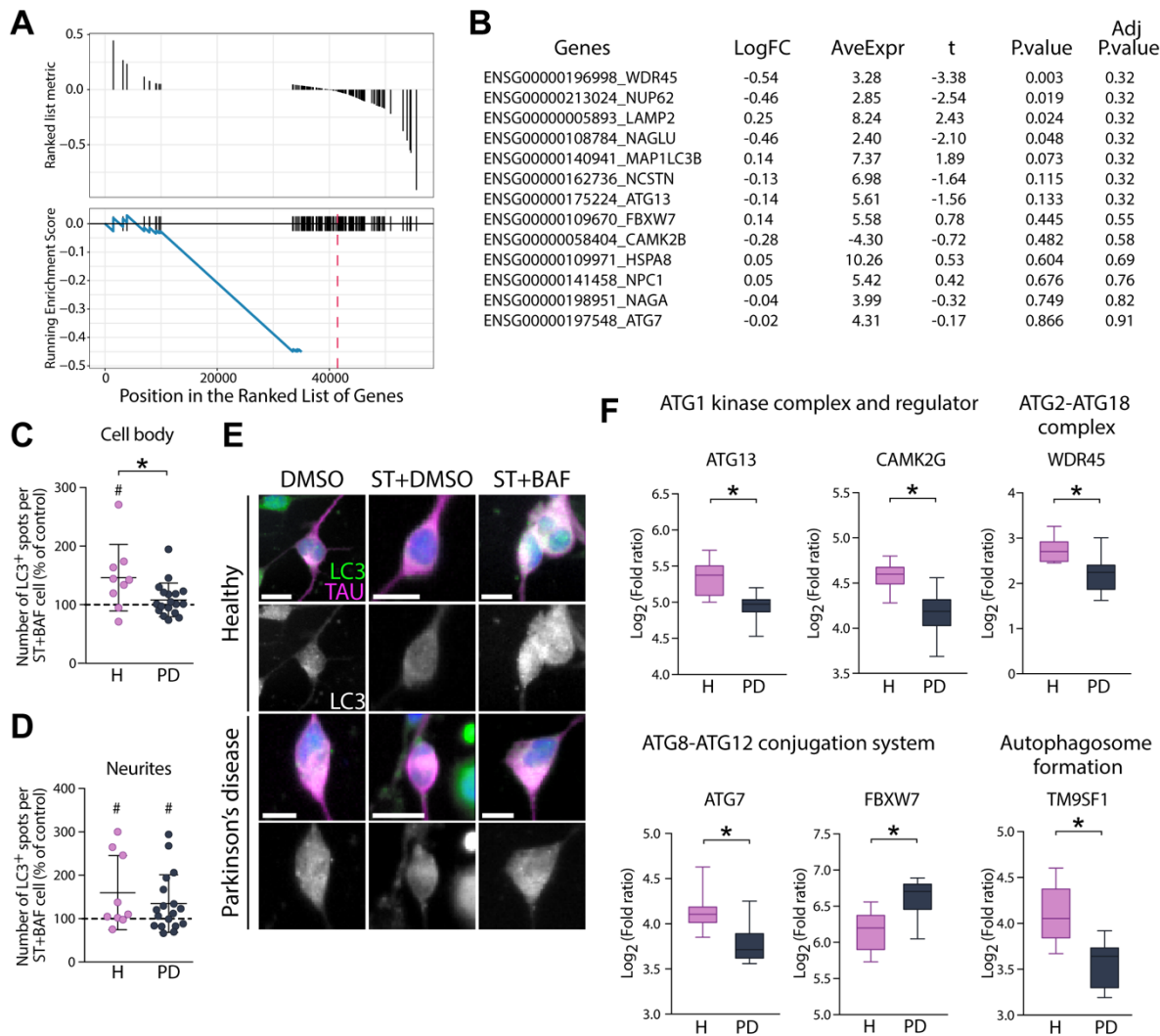


Figure S9. PD-iNs do not accumulate autophagosome structures following impairment of autophagy.

(A) GSEA plot of the “LYSOSOME” KEGG pathway in PD-iNs (Adj.P.Val = 0.028).

(B) LogFC and P. value table of autophagy and lysosome related genes in parental fibroblasts. Negative logFC means down-regulated in PD. Adj.P.Val” represents the P.value after transcriptome wide adjustment with the FDR method. (n=10 healthy and n=10 PD lines).

(C) Quantification of LC3-positive puncta in the cell body of TAU-positive iNs (mean average of 425 TAU-positive cells assessed per line, n=9 healthy and n=18 PD lines). Kolmogorov-Smirnov test: *P=0.0493, D=55.56. Two-tailed Wilcoxon matched pairs signed rank test, #P=0.0371.

(D) Quantification of LC3-positive puncta in the neurites of TAU-positive iNs (mean average of 425 TAU-positive cells assessed per line, n=9 healthy and n=18 PD lines). H: two-tailed Wilcoxon matched pairs signed rank test, #P=0.0371, PD: two-tailed paired t-test: #P=0.0499, df=16.

(E) LC3-positive dot expression and spot detection analysis in TAU-positive iNs. Scale bar = 10µm.

(F) Boxplots of log₂ fold changes in expression of genes associated with autophagy (n=10 healthy and n=10 PD lines) (adjusted P value < 0.05).

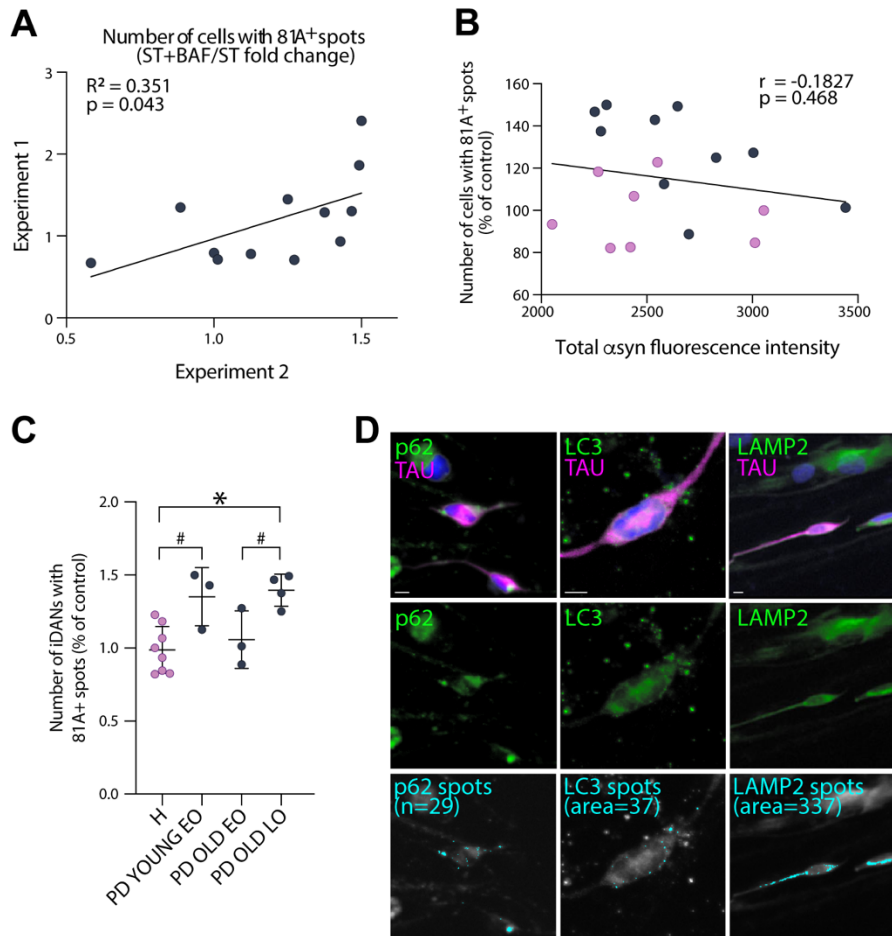


Figure S10. Autophagy impairments lead to an accumulation of phosphorylated asyn in PD-iDANs.

(A) Reproducibility of the experiment shown in Figure 6c,d as assessed by a positive correlation between the number of iNs with 81A-positive puncta between two independent experiments (different lentiviral batches, passage number of the parental fibroblasts, laboratory in which they were done as well as the experimenter performing the experiments and the quantifications), showing that the same cell line show 81A-positive puncta accumulation independently of the experimental conditions. Pearson's correlation: $P=0.043$; 95% confidence interval: 0.02770 to 0.8703.

(B) No association between the number of 81A-positive puncta and the total asyn fluorescence intensity in iDANs ($n=18$ lines). Spearman's rank correlation: $P=0.468$; 95% confidence interval: -0.6080 to 0.3242.

(C) Differences in the number of iDANs with 81A-positive puncta depending on the age of the PD patient and their age at onset. Young EO: patients younger than 60 years of age, with disease onset before years of age. Old EO: patients older than 60 years of age, with disease onset before 60 years of age. Old LO: patients older than 60 years of age, with disease onset after 60 years of age. One-way ANOVA: $*P = 0.0458$. Unpaired t-test: $\#P < 0.05$.

(D) p62-positive, LC3-positive dans LAMP2-positive puncta expression in TAU-positive cells with the most elevated values of puncta quantification. Cyan overlay represents the puncta that were quantified for analysis. Abbreviations: BAF: bafilomycin A1; EO: early onset; H: healthy; LO: late onset; PD: Parkinson's disease, ST: starved.

Supplemental Table

Table S1. List of Antibodies

| Antibody | Source | Species | Dilution | Catalogue number | Antibody registry number or PMIDs |
|--------------------------------------|--|---------|-----------------------------|------------------|--|
| 81A | Gift from Kelvin Luk, University of Pennsylvania | Mouse | 1:10 000 | NA | 24931606 , 24659240 , 25732816 |
| | Abcam | Mouse | 1:500 | Ab184674 | AB 2819037 |
| Alpha-synuclein | Abcam | Chicken | 1:1 000 | Ab190376 | AB 2747764 |
| Aldh1a1 | Abcam | Rabbit | 1:200 | Ab23375 | AB 2224009 |
| Collagen 1 | Abcam | Rabbit | 1:1 000 | Ab34710 | AB 731684 |
| GFAP | Millipore | Mouse | 1:1 000 | MAB3402 | AB 94844 |
| Anti-Histone H2A.X, phospho (Ser139) | Millipore | Mouse | 1:500 | 05-636 | AB 309864 |
| HSC70 | Abcam | Rat | ICC: 1:2 000 WB: 1:5 000 | Ab19136 | AB 444764 |
| | Thermo Scientific | Mouse | 1:100 | MA3-014 | AB 325462 |
| LAMP2 | DSHB | Mouse | 1:100 | H4B4 | AB 528129 |
| LAMP2a | Abcam | Rabbit | ICC: 1:1 000 WB: 1:2 000 | Ab18528 | AB 775981 |
| LC3B | Sigma | Rabbit | ICC: 1:500 WB: 1:5 000 | L7543 | AB 796155 |
| MAP2 | Abcam | Chicken | 1:10 000 | Ab5392 | AB 2138153 |
| P62 | Abcam | Rabbit | ICC: 1:500 WB: 1:5 000 | Ab91526 | AB 2050336 |
| TAU HT7 | Thermo Fisher Scientific | Mouse | 1:500 | MN1000 | AB 2314654 |
| TAU | Agilent Technologies | Rabbit | 1:500 | A0024 | AB 10013724 |
| TH | Millipore | Sheep | 1:1 000 | Ab1542 | AB 90755 |
| VMAT2 | Sigma | Rabbit | 1:200 | AB1598P | AB 2285927 |

Reference

Caiazzo, M., Dell'Anno, M. T., Dvoretzkova, E., Lazarevic, D., Taverna, S., Leo, D., Sotnikova, T. D., Menegon, A., Roncaglia, P., Colciago, G., Russo, G., Carninci, P., Pezzoli, G., Gainetdinov, R. R., Gustincich, S., Dityatev, A., and Broccoli, V. (2011). Direct generation of functional dopaminergic neurons from mouse and human fibroblasts. *Nature* 476, 224-227.